

Jurassic–Cretaceous deformational phases in the Paraná intracratonic basin, southern Brazil

Abstract

This paper examines the domes and basins, regional arcs and synclines, and brittle structures in upper units of São Bento Group (of the Paraná Basin) flood volcanism to characterize the deformational phases in its Jurassic to Cretaceous history. Geometric, kinematic and dynamic structural analyses were applied to define First-stage fieldwork revealed brittle structures, extensional joints, and strike-slip faults, and second stage fieldwork investigated the connections of the brittle structures to both open folds and dome and basin features. Fault-slip data inversion was performed using two different techniques to distinguish local and remote stress/strain. Geometric and kinematic analyses completed the investigations of the deformation, which characterized two deformational phases, for the Jurassic to Cretaceous periods in the Paraná Basin. Both developed under regional bi-directional constrictional ($\sigma_1 \geq \sigma_2 \gg \sigma_3$) stress regimes that produced a number of non-cylindrical folds. The D1 deformational phase produced the N–S and E–W orthogonally oriented domes and basins. The D2 arcs and synclines are oriented towards the NW and NE and indicate a clockwise rotation (35–40°) of both horizontal principal stress tensors. Stress/strain partition in elongated domes or basins controls lower scale structural elements distribution. The extensional joints and strike-slip faults characterize the local stress field in the outer rim of the orthogonally buckled single volcanic flow, whereas the inner rim of the buckled single flow supported constriction and thus, developed the local arcuate folds. Fault-slip data inversion was performed using two different techniques to distinguish local and remote stress/strain. The strike-slip is then a local scale stress regime, resulting from stress drop after the onset of extensional joints (orthogonal dykes patterns) in the outer rim of domes or basins.

1

2

1
2
3
4
5
6
7
8
9
10
11
12
13
14
15
16
17
18
19
20
21
22
23
24
25
26

1 Introduction

The Paraná Basin is located in the South America Plate (Fig. 1) and is characterized as a huge Paleozoic to Mesozoic intracratonic depression filled by sedimentary and volcanic rocks (see Zalán et al., 1991; [and Zalán, 2004 for a revision on stratigraphy and tectonic subjects](#)). [The upper stratigraphic sequences \(São Bento and Guará groups\) occupy c.a. 80% of the basin area. The São Bento Group is mainly composed by Serra Geral Formation, which contains the volcanic rocks of the well-known Paraná–Etendeka Flood Basalt Province \(Wilson, 1989\).](#) However, ~~t~~The regional stratigraphic correlation and facies change for the ~~uppermost sequences in the Paraná Basin (São Bento Group)~~ remain controversial, since Scherer and Lavina (2006) correlated the Pirambóia Fm. with Neo-Permian sedimentary units, while Soares et al. (2008a) correlated it with Neo-Triassic to Jurassic sedimentary units. The regional isopach maps for the Mesozoic sedimentary sequence (Artur and Soares, 2002; Soares et al., 2008b) fit well with the results presented here. Thus, the proposition by Soares et al. (2008a) is adopted to characterize the Jurassic–Cretaceous stratigraphic interval of the Paraná Basin. As a result, the São Bento Group is considered to comprise the Pirambóia and Guará (Eo to Meso-Jurassic), Botucatu (Neo-Jurassic), and Serra Geral (Cretaceous) formations (Soares et al., 2008a). ~~The Serra Geral Formation is mainly composed of volcanic rocks, well known as the Paraná–Etendeka Flood Basalt Province (Wilson, 1989).~~

The main structural features of the Paraná Basin were recognized using satellite imagery lineaments and fault plane trends (e.g., Soares et al., 1982; Zerfass et al., 2005; Reginato & Strieder, 2006; Strugale et al., 2007; Machado et al., 2012; Nummer et al., 2014; Jacques et al., 2014), geophysical lineaments (e.g., Ferreira, 1982; Ferreira et al., 1989; Quintas, 1995), or isopach maps developed for each sedimentary sequence (e.g., Northfleet et al., 1969; Artur and Soares, 2002). The main findings include regional lineaments, arcs, and flexures (Fig. 1) that have been summarized by Almeida (1981), Zalán et al. (1991), and Zalán (2004). These

1 authors also highlighted the influence of the basement on the development of these structural
2 features in the Paraná Basin. These regional-scale structural features deform the entire Paraná
3 Basin sequence and do not depend on the stratigraphic interpretation of the uppermost
4 sequences.

5 Riccomini (1995) conducted the first paleostress investigation of the uppermost stratigraphic
6 units of the Paraná Basin by applying the method of Angelier and Mechler (1977). Due to the
7 large predominance of the lateral fault-slip data, Riccomini (1995) adopted a strike-slip stress
8 regime to ~~and distinguished~~ a number of deformational phases from the Permian units of the
9 Paraná Basin through to the Holocene continental margin rift basins (Table 1) ~~by applying the~~
10 ~~method of Angelier and Mechler (1977)~~. The main criterion ~~used~~ to distinguish the
11 deformational phases was, then, to separate fracture direction families with compatible sense
12 of movement. These assumptions and procedures ~~Riccomini (1995) interpreted these~~
13 ~~deformational phases by considering transeurrent regimes, mainly due to the large~~
14 ~~predominance of striae parallel to the fault strike and~~ were based on propositions suggesting
15 differential movements during South American and African plate rotation after Gondwana
16 rifting (Morgan, 1983; Chang et al., 1992; Riccomini, 1995).

17 Recent publications also adopted a strike-slip stress regime, following the proposition of
18 Riccomini (1995).~~ly~~, Strugale et al. (2007) distinguished two deformational phases in the
19 Jurassic and Cretaceous of the Ponta Grossa Arc region. These deformational phases can be
20 correlated to D_{n+1} and D_{n+2} described by Riccomini (1995). Similarly, Machado et al. (2012)
21 and Nummer et al. (2014) distinguished three deformational phases in the high hills of the
22 Torres Syncline. These phases can also be correlated with the D_n , D_{n+1} , and D_{n+2} phases
23 proposed by Riccomini (1995).

24 Heemann (1997, 2005), Reginato (2003), Acauan (2007), and Amorim (2007) also applied the
25 Angelier and Mechler (1977) method to fault slip data from volcanics and interlayered aeolian

1 sandstones of the Serra Geral Fm. ~~However, the~~ seir works, ~~which involved a~~ adopted
2 geometric and symmetry analysis of fault slip data ~~to~~, ~~enabled deformational phases to be~~
3 ~~distinguished. Consequently, Heemann (1997, 2005), Reginato (2003), Acauan (2007), and~~
4 ~~Amorim (2007) distinguished~~ two deformational phases: i) a NS and EW oriented stress field,
5 and ii) a NW and NE oriented stress field; ~~however~~ but, ~~they could not determine which of~~
6 ~~these was the first.~~ However, some of the observed structural features do not equate for a
7 strike-slip stress regime. Strieder and Heemann (1999) and Reginato and Strieder (2006)
8 highlighted the NS–EW orthogonal pattern of the sandstone dikes and mineralized veins
9 emplaced into the basalts. Heemann (1997, 2005), Reginato (2003), Acauan (2007), and
10 Amorim (2007) also identified areas with opposite positioning of the maximum and minimum
11 stress axes (Table 2), ~~although their findings were difficult to interpret.~~ Therefore, these
12 results were under evaluation ~~need to be investigated further using~~ and -additional fieldworks
13 for fault slip data, ~~and~~ fault geometry analysis and arcuate fold analysis were carried out.
14 The present paper aims to demonstrate that a bi-directional constrictional stress state regime
15 was active during Jurassic (Botucatu Fm.) and Cretaceous (Serra Geral Fm.) periods in the
16 Paraná Basin. This
17 ~~study aimed to reports the results of a large scale structural analysis survey conducted within~~
18 ~~the Serra Geral and the underlying Botucatu formations. An analysis of the brittle structures~~
19 ~~focused mainly on stress inversion techniques applied to fault slip data from volcanic rocks in~~
20 ~~order to distinguish the different phases of deformation and evaluate the paleostress field~~
21 ~~during the Jurassic to Cretaceous periods.~~
22 ~~The paper presents a geometrical and kinematical analysis of mesoscale faults (10–100 m~~
23 ~~long) investigatstudied at 42 sites (quarries and large road cuts) located within the central~~
24 ~~region and eastern border of the Paraná Basin.~~ This stress state regime was determined by
25 means of structural analysis techniques from e symmetry, geometric, kinematic and dynamic

1 ~~analysis incorporate or constrain their times of occurrence,~~ a number of local and regional
2 structural elements used ~~were used~~ to characterize these deformational phases: ~~fault plane,~~
3 ~~slip direction and sense, type of kinematic indicator, fault splay geometry, fracture opening~~
4 ~~and infilling, large scale folding and dome and basin features, and the basal contact of the~~
5 ~~Botucatu and Serra Geral formations.~~

6 The structural analysis follows Turner & Weiss (1963, p. 3-11). The geometric analysis is
7 developed for outcrop and regional scale folds, domes and basins, and also for fractures
8 (joints and faults). The kinematic analysis is based on paleostress inversion, but its results are
9 reconciled with geometry and symmetry of fractures. The dynamic analysis of the
10 deformation integrates geometric and kinematic analyses for both folds and fractures, in order
11 to define the deformational regime, the structural relationships between folding and
12 fracturing, and, finally, stress drop and tensor permutation, and the development of orthogonal
13 joint pattern.

14
15 ~~The paper also discusses the stress state regime tectonic conditions within which the~~
16 ~~paleostress axis inversion operated and the orthogonal joint pattern developed. In this way,~~
17 ~~the dynamic analysis discusses the operation of local and far (remote) stress field in~~
18 ~~development of the structural elements. Orthogonal joint formation and its associated stress~~
19 ~~inversion remain subjects of discussion, and a number of mechanisms have been proposed to~~
20 ~~account for the local and regional deformational features (see Caputo, 1995; Caputo and~~
21 ~~Hancock, 1999; Bai et al., 2002). Based on these elements, the mesoscale fault geometries~~
22 ~~and fault slip data of the rocks of the Serra Geral Fm. have been shown to be reliable~~
23 ~~indicators of the distribution of the local paleostress state in the Paraná Basin during the~~
24 ~~Jurassic to Cretaceous periods.~~

25

2 Fieldwork and structural analysis methods

The fieldworks were carried out in three research stages to ~~The regularities of the preliminary paleostress fields~~ recorded structural features in the volcanic rocks and intertrap sandstones of the Serra Geral Fm., and in the Botucatu Fm. sanstones, mainly at the contact of these formations. The investigated structural features include: fault plane, slip direction and sense, type of kinematic indicator, fault splay geometry, fracture opening and infilling, fold of different scales and dome-and-basin features, and the basal contact of the Botucatu and Serra Geral formations. ~~at different sites inspired a second stage of fieldwork, which involved both revisiting previous sites to obtain a more complete structural study and surveying new sites in the southern Paraná Basin.~~

~~A third stage of fieldwork was performed to characterize the gentle folds and dome and basin structures developed within the Botucatu and Serra Geral formations. The procedure for characterizing such structures involved their identification from satellite imagery or aerial photographs, followed by fieldwork to measure the sandstone-basalt contact orientations, or the basal surface of a given basalt flow.~~ The significance of fault-slip data on this study makes necessary to show explicitly i) the field analysis for splaying Riedel fractures geometry and symmetry and the recorded type of striae, and ii) the paleostress technique used for fault-slip data inversion.

2.1. Fieldwork methods for brittle structures

The ~~structural-geological studies were undertaken~~ brittle structural features were investigated in open-pit quarries, underground openings, and large road cuts (mesoscale faults: 10–100-m long). ~~This~~ investigation were carried out of the brittle structures from the in 42 sites, and involved analysis of the slip direction and sense of movement of more than 800 fault planes. To ensure the confidence of the results, only those records with a clearly defined slip sense

1 were sampled for the computation of the paleostress fields. Brittle structures were recorded in
2 basalts, andesites and dacites of the Serra Geral Fm., since kinematic indicators are best
3 preserved in these lithologies.

4 Field investigations also included geometrical data records based on fracture splaying (Fig. 2).
5 Fracture splaying shows patterns similar to synthetic and antithetic fractures developed during
6 shear experiments (e.g., Tchalenko, 1970; Tchalenko and Ambraseys, 1970). Most fracture
7 patterns exhibit open spaces and at least one of those fractures is mineralized. ~~Mineralization~~
8 ~~is composed of carbonate, chalcedony, and zeolites, or a combination of~~
9 ~~carbonate + chalcedony + celadonite.~~ The fracture patterns, ~~and~~ mineralization of dilatational
10 spaces and sandstone dikes can be observed on different scales, but their geometric
11 relationships are more easily distinguished on the outcrop scale. A field diagram was
12 developed to compile and record different fracture patterns (Fig. 3).

13 Kinematic indicators include a variety of types, but frictional steps and the accretionary
14 growth of crystal fibers (Hancock, 1985), and RM and TM types of secondary fracture steps
15 (Petit, 1987) largely predominate (Fig. 4). Some fault planes display different slip striations
16 and movements, and occasionally crosscutting (truncation) relations could be recorded (Fig.
17 4B). The truncation between different striations in the same plane suggests their age relation
18 (Table 3). A rare melted and polished fault plane with slip striae is shown in Fig. 4C and
19 ductile drag deformation of the horizontal joints can be observed in Fig. 4D in the basaltic
20 rock with the development of a fracture cleavage.

22 **2.2. Methods for evaluation of deformational phases in the Serra Geral Fm.**

23 The first approximations for paleostress regimes in the volcanic rocks of the Paraná Basin
24 used the graphical method described by Angelier and Mechler (1977). This graphical method
25 superposes P and T dihedrals for each element of fault-slip data, which allows paleostress

1 regimes to be distinguished by grouping compatible fracture splay geometries and fault slip
2 data.

3 In the second phase of the paleostress analysis, the above graphical method was combined
4 with ~~two~~ numerical stress-inversion techniques (Žalohar and Vrabc, 2007, 2008), by means
5 of the T-TECTO 3.0 program (http://www2.arnes.si/~jzaloh/t-tecto_homepage.htm)
6 developed by Dr. Jure Žalohar. The Gauss method is an inverse-method that is applied to
7 define paleostress (Žalohar and Vrabc, 2007), whereas the MSM is used as the direct
8 kinematic paleostrain method (Žalohar and Vrabc, 2008). The parameters for stress inversion
9 by MSM are shown in Table 4.

10 The Gauss method was applied site-by-site to limit the fault-slip data numbers and to evaluate
11 local heterogeneities in the paleostress regimes of the Paraná Basin volcanic rocks. It is
12 important to note that the Gauss method can distinguish between heterogeneous fault-slip
13 data, as is the present case (two superposed deformational phases). ~~The separation of~~
14 ~~paleostress regimes from heterogeneous fault systems is tedious. In the present case, the~~
15 ~~complete fault slip data sets were tested by applying the Gauss method described by Žalohar~~
16 ~~and Vrabc (2007). This method defines a Gaussian compatibility function based on the~~
17 ~~adjustment measure between the angular misfit and the normal to the shear stress ratio on the~~
18 ~~fault plane. The Gauss method proposed by Žalohar and Vrabc (2007) can distinguish~~
19 ~~between heterogeneous fault slip data, as is the present case.~~

20 ~~Then, the Gauss method was applied site-by-site to limit the fault slip data numbers and to~~
21 ~~evaluate local heterogeneities in the paleostress regimes of the Paraná Basin volcanic rocks.~~

22 In order to obtain numerically stable results, the fault-slip data of some sites were merged
23 based on their proximity, fault-slip consistency, geometry, and fault pattern. The merged
24 fault-slip data represent small areas of the Paraná Basin under homogeneous stress/strain

1 conditions. These fault-slip data were then reprocessed and the results used for the structural
2 analysis discussion.

3 ~~The stress inversion was performed using the T TECTO 3.0 program~~
4 ~~(http://www2.arnes.si/~jzaloh/t_tecto_homepage.htm) developed by Dr. Jure Žalohar. The~~
5 ~~paleostress/paleostrain regimes were determined using the Gauss method and kinematic~~
6 ~~multiple slip method (MSM) (Žalohar and Vrabc, 2008). The MSM calculates weighting~~
7 ~~factors for moment tensor summation based on the number and orientation of parallel faults of~~
8 ~~the same size range, direction of slip along them, and the mean rock properties. The~~
9 ~~parameters for stress inversion by MSM are shown in Table 4.~~

10 ~~The reduced tensors calculated by these methods can be interpreted either as the stress or~~
11 ~~strain tensor. The Gauss method is an inverse method that is applied to define paleostress~~
12 ~~(Žalohar and Vrabc, 2007), whereas the MSM is used as the direct kinematic paleostrain~~
13 ~~method (Žalohar and Vrabc, 2008).~~

14 **3 Regional structural features in the Jurassic–Cretaceous units of the Paraná** 15 **Basin**

16 Figure 1 shows some structural features that affect the stratigraphic units of the entire Paraná
17 Basin; however, some are of particular interest with regard to the Jurassic–Cretaceous interval
18 because it will be shown here that they were developed during the deformational phases.

19 The most prominent structures are the large-scale anticlinal and synclinal gentle folds in the
20 eastern border of the Paraná Basin (Fig. 5), which show NW-dipping hinges (see Zalán et al.,
21 1991). Erosion of the anticlines created the area in which the volcanic and sedimentary rocks
22 of the Paraná Basin are exposed towards the NW, and gave rise to the Rio Grande and Ponta
23 Grossa arcs. However, the folds are not cylindrical, but produce elliptical domes and basins
24 (details in Fig. 5).

1 The presence of large domes in the Serra Geral volcanics has long been reported (e.g., Lisboa
2 and Schuck, 1987; Schuck and Lisboa, 1988; Rostirolla et al., 2000). Similar structures were
3 also described for underlying sedimentary sequences (Riccomini, 1995). Close examination of
4 these structural features reveals that they are an association of gentle domes and basins, which
5 can be classified into two groups based on orientation: a) those with N–S or E–W ~~orientation~~,
6 and b) those with NW or NE for the longest axis direction~~orientation~~. Some examples of such
7 domes are indicated in Fig. 5: a) Quaraí Dome, b) Rivera Crystalline Island, and c) Aceguá
8 Crystalline Island. The longest axis of these domes is <100 km. The Quaraí Dome shows a
9 NE orientation of its longest axis, while the Rivera and Aceguá crystalline islands exhibit EW
10 orientation. Aboy and Masquellin (2013) presented some structural and sedimentary evidence
11 supporting the uplift of the Rivera Crystalline Island from the Permian period onwards.

12 The basal contact of the Serra Geral Fm. volcanic rocks was measured in a number of
13 outcrops to constrain the deformation related to the NW-dipping anticlines–synclines (Fig.
14 5A). Figure 5B shows that the axes of these continental-scale gentle folds are oriented
15 towards 06/308. A balanced SW–NE structural section (Fig. 6) illustrates the relationships
16 between the anticlines–synclines from Uruguay to São Paulo (Brazil). This regional cross
17 section was balanced as concentric folds (Marshak and Mitra, 1988; pp. 269–302).

18 Structural mapping was conducted in the Quaraí Dome area, close to the Brazil–Uruguay
19 border (Fig. 7A). In this area, the erosion of volcanic flows over the Botucatu Fm. sandstones
20 allows a number of domes and basins with different orientations to be recognized. The most
21 important of these is the Quaraí Dome, because it has the greatest amplitude and it exposes
22 the underlying Botucatu Fm. sandstone. Measurements of the sandstone–basalt contact show
23 that the Quaraí Dome is oriented towards 02/043 (Fig. 7B).

1 North and northwest of the Quaraí Dome, two elongated basins (N–S and E–W, respectively)
2 can be recognized (Fig. 7A). The attitudes of the thin volcanic flows are shown for the E–W-
3 dipping (Fig. 7C) and N–S-dipping (Fig. 7D) long axes for both basins.
4 The N–S-oriented folds were also recognized on the outcrop scale (Fig. 7E). This fold is
5 developed upon the Botucatu Fm. sandstone and it was identified in the inner part of the
6 Quaraí Dome along the BR-293 road. The eolian stratification was deformed around an
7 11/176 folding axis (Fig. 7F).
8 The map in Fig. 7A shows that the domes and basins with the same orientation do not
9 interfere with each other. The folds are described as non-cylindrical and arcuate in map view.
10 The fold tightness varies from gentle (interlimb angle: 170° for small domes and basins, 151°
11 for the Quaraí Dome, and 159° for regional arcs) to open fold (interlimb angle: 120° for the
12 N–S outcrop fold).

13

14 **4. Paleostress tensors in the Serra Geral Fm. volcanic rocks**

15 The results of the fault-slip data processing are presented in a sequence of figures for each
16 site/area (Figs. 8 and 9). The figures include the Wulff projection (lower hemisphere) of the
17 brittle fault-slip data, misfit angle histogram, unscaled Mohr diagram for resolved stress on
18 the faults, and a diagram relating the values for the object function (M) and shape of the strain
19 ellipsoid (D). The object function depends on the parameters defined in Table 4, and relates
20 the standard deviation (s) of angular misfit between the direction of slip along the faults
21 (striae) and the shear stress produced by a given tensor. Therefore, its value is used to
22 determine the best orientation of stress tensor for those fault-slip data (Žalohar and Vrabc,
23 2007).

24 The structural analysis performed on the Serra Geral Fm. volcanic rocks (Paraná Basin)
25 distinguished two different paleostress fields:

- 1 a) Predominantly N–S-oriented maximum horizontal stress with permutations to the E–
2 W;
3 b) Predominantly NE–SW-oriented maximum horizontal stress with permutations to the
4 NW–SE.

5 In both cases, the intermediate principal stress (σ_2) is subvertical, which explains the
6 prevalence of strike-slip faulting. The crosscutting relations between striations (Table 1)
7 indicate that the N–S maximum horizontal stress is older than the NE–SW stress. This
8 interpretation is also consistent with other structural features such as the elliptical domes.

9 ~~These general orientations for the NE–SW (NW–SE) stress tensors agree with those presented~~
10 ~~by Riccomini (1995), Strugale et al. (2007), Machado et al. (2012), and Nummer et al. (2014).~~
11 ~~They differ, however, on processing methodology and kinematic analysis. It should be noted~~
12 ~~that the area studied by Riccomini (1995) and Strugale et al. (2007) is heavily influenced by~~
13 ~~the NW–SE Ponta Grossa faults and dikes. Despite final results that are difficult to reconcile,~~
14 ~~it seems that the D1 faults (deformation) defined by Strugale et al. (2007) correspond to the~~
15 ~~D2 deformational phase discussed here.~~

16

17 **4.1. Predominantly N–S-oriented maximum horizontal stress with permutations** 18 **to the E–W**

19 The maximum (σ_1) and minimum (σ_3) compressive paleostresses are subhorizontal (Fig. 8).
20 These main paleostress axes are oriented close to the N–S and E–W directions and in most
21 cases, the stress ratio (Φ) ranges from 0.10–0.30. The mean misfit angle of the fault-slip data
22 for each site/area is $<15^\circ$ (see Fig. 8), while the standard deviation is $<20^\circ$ (see Table 5).
23 These conditions suggest a strike-slip regime and the observed fault-slip data indicate the
24 presence of conjugate patterns of faults (Fig. 8).

1 This group of tensors shows the permutations of the maximum (σ_1) and minimum (σ_3)
2 compressive paleostress axes between the N–S and E–W directions. In Fig. 8(A, B, E, and G),
3 the maximum compressive (σ_1) paleostress axis is close to the E–W direction, whereas in Fig.
4 8(C, D, F, H, and I), the maximum compressive (σ_1) tensor is close to the N–S direction. Such
5 results, recorded in the CODECA quarry (Fig. 6G and 6H), were initially intriguing and
6 demanded a careful re-investigation of the fault-slip at this site. The alternated orientation of
7 the maximum paleostress axis was observed at other sites/areas within the Paraná Basin
8 volcanic rocks. Furthermore, the alternation of the stress tensor occurs in some tectonic
9 regimes (Angelier, 1989) and this aspect will be considered later.

10

11 **4.2. NE–SW maximum horizontal compression**

12 This group of paleostress tensors is also related to the subhorizontal maximum and minimum
13 compressive stresses, while the intermediate stress axis (σ_2) is subvertical (Fig. 9). The
14 maximum horizontal compressive stress is oriented close to NE–SW and the stress ratio (Φ)
15 ranges from 0.10–0.30. These conditions also suggest a strike-slip stress regime and the
16 presence of a conjugate pattern of faults (Fig. 9).

17 The mean misfit angle of the fault-slip data for each site/area is close to 15° (see Fig. 7) and
18 the standard deviation is $<18^\circ$ (see Table 6). Table 6 summarizes the results of the stress
19 inversion for this fault-slip data set.

20 The paleostress tensors also indicate the permutations between the maximum (σ_1) and
21 minimum (σ_3) compressive stress axes from the NE–SW to NW–SE directions in some
22 sites/areas (Santa Rita quarry) (see Fig. 9A–F).

23

24 **5. Geometric and kinematic analyses of deformational structures in the** 25 **volcanic rocks**

1 The regional-scale folds (Fig. 5) and the domes and basins (Fig. 7) discussed in the previous
2 sections show systematic relationships with the fracture patterns (Figs. 8 and 9). Thus, the
3 deformational structures developed within the volcanic rocks of the Serra Geral Fm. are
4 analyzed considering the fracture patterns.

5 The geometric and kinematic analyses of fracture patterns use rose diagrams to classify
6 conjugated and splay fractures observed in each site/area, because the strike-slip stress regime
7 developed subvertical to vertical fractures. This procedure makes it possible to distinguish the
8 synthetic and antithetic fractures and to determine the mean ϕ (internal friction angle; see
9 Jaeger, 1969; Angelier, 1989).

10

11 **5.1. Fracture patterns of N–S paleostress tensors**

12 The fracture patterns developed in the N–S maximum horizontal compression clearly indicate
13 conjugate geometry, as can be seen in Fig. 10. However, it is clear that dextral and sinistral
14 conjugate sets show different spatial distributions (orientations) and frequency.

15 The rose diagrams in Fig. 10 show fracture orientations according to the synthetic Riedel
16 fracture criteria (Tchalenko 1970) and reinforce the field observations (Fig. 2). The rose
17 diagrams indicate the predominance of R-type fractures and some diagrams illustrate the
18 presence of fractures at angles lower than 15–20° relative to the main compressive stress axis
19 (σ_1). These fractures are classified as hybrid joints (Hancock, 1985).

20 R-type fractures usually merge with C-type fractures to develop splay or duplex fracture
21 patterns, and hydraulic breccia are often associated with such dilatational spaces. The
22 dilatational space is filled by a zeolite \pm quartz \pm chalcedony \pm calcite \pm celadonite
23 paragenesis.

24 The geometric and kinematic analyses of the N–S-directed paleostress field also consider the
25 occurrence of tabular dykes of thermally metamorphosed sandstone emplaced into the

1 vesicular basalts (Fig. 11A) of the Serra Geral Fm. sequence. A detailed field survey of their
2 orientation was undertaken in the Salto do Jacuí region. Figure 11B shows that these tabular
3 dykes are predominantly subparallel to the maximum compressive stress axis (σ_1) when it is
4 oriented either to the N–S or to the E–W.

5 In the Caxias do Sul region, the thermally metamorphosed sandstone tabular dykes were
6 measured cutting across the massive basalts of the Serra Geral Fm. Figure 11C shows that
7 such dykes are also oriented to the NE–SW; however, they still show the main distribution in
8 the N–S and E–W directions. In the Caxias do Sul region, a large number of mineralized veins
9 were measured. Figure 11D shows that opened fractures are mainly oriented in the N–S, E–
10 W, and NW–SE directions.

11 The orientation of metamorphosed sandstone dykes in the Salto do Jacui and Caxias do Sul
12 regions are slightly different. For the Salto do Jacui region, the preferred orientation is N10E,
13 whereas in the Caxias do Sul region, it is N10W. However, such differences are in accordance
14 with the local stress field orientations, as can be seen in Fig. 8(C, D, E, G, and H).

15 The sandstone dykes and mineralized veins cutting across the basalts are controlled by an
16 orthogonal pattern of fractures. This observation agrees with the permutations of the
17 maximum (σ_1) and minimum (σ_3) compressive paleostress axes between the N–S and E–W
18 directions, as reported above.

19 This orthogonal pattern (N–S and E–W) is also observed in the Cerro do Jarau giant intertrap
20 dune (Remde, 2013). The orthogonal pattern in the Cerro do Jarau area (Fig. 7A), however, is
21 defined by centimeter-scale veins in the basalts (Fig. 12A), and mainly by millimeter-scale
22 deformation bands in the intertrap Botucatu Fm. sandstone (Fig. 12B). The centimeter-scale
23 veins in the basalts display a “ladder” pattern, or an H-shaped abutment (Hancock 1985),
24 where the N–S veins are longest. In contrast, the deformation bands display a “grid” pattern
25 with mutual crosscutting relationships (Rives et al., 1994). The orthogonal deformation bands

1 are crosscut by shear deformation bands (Fig. 12C), suggesting an initial onset of extensional
2 joints, followed by shear. Figure 12(D and E) shows the rose diagrams for the orthogonal
3 patterns in the basalt and sandstone, respectively, in the Cerro do Jarau area.

4

5 **5.2. Fracture patterns of NE–SW-directed paleostress field**

6 The geometry of the fractures formed in the NE–SW-directed paleostress field shows an
7 asymmetric distribution for the dextral and sinistral conjugated branches (Fig. 13). This
8 asymmetric distribution of fracture orientation frequency allows them to be classified
9 according to the Riedel shear criteria. However, the fault-slip data for the NE–SW paleostress
10 field show that higher frequency Riedel fractures vary between sites, being classified as either
11 R-type, C-type, P-type, or even hybrid fractures.

12 The rose diagrams for the NE–SW paleostress field are in accordance with field observations
13 of fracture splaying. The R- and C-type fractures usually merge into one another to produce
14 both dextral or sinistral splayed fractures and duplex strike-slip patterns. Such fracture
15 patterns are the locus for mineralization. Fracture surfaces and open dilatational spaces are
16 coated by celadonite ± chalcedony ± calcite. Hydraulic breccias are also recognized, but with
17 minor frequency.

18 Some rose diagrams in Fig. 13 indicate the presence of extension to the hybrid joints
19 (Hancock, 1985) and additionally, Fig. 13(E and F) suggests the development of the
20 orthogonal fracture pattern in this second deformational phase. In the Cerro do Jarau giant
21 intertrap dune (Fig. 7A), the N–S orthogonal deformation bands are also superposed by “grid”
22 patterns of orthogonal NE–SW deformation bands (Fig. 14A). Careful measurement and
23 evaluation of the orthogonal patterns at a number of outcrops permitted the construction of a
24 rose diagram for this second generation of deformation bands (Fig. 14B). The dispersion of

1 the orthogonal NE–SW deformation bands also suggests the interplay of extensional and
2 hybrid joints.

3

4 **6. Stress/strain regime aAnalysis of the deformational phases**

5 The paleostress analysis distinguished two different deformational phases in the upper units of
6 the São Bento Group ~~Serra Geral Fm. volcanic rocks~~ (Paraná Basin). The relative ages of the
7 deformational events were established from field observations (Table 1), regional-scale folds
8 (Fig. 5), and domes and basins (Fig. 7). The N–S-oriented stress field was assessed as being
9 older than the NE–SW-oriented stress field deformational phase during the Jurassic to
10 Cretaceous periods.

11 The regional-scale folds and the dome-and-basin features (Figs. 5 and 7) were shown to
12 pertain to two distinct groups: i) those with N–S and E–W elongations, and ii) those with NE
13 and NW elongations. These directions are closely related to that determined for the
14 orthogonal fracture patterns and faults in the previous sections. Considering Figs. 5, 7–10, 12,
15 and 13, it can be established that a relationship of symmetry exists between the fractures,
16 faults, and folds of the elongated domes and basins. Thus, the association between buckling
17 processes and brittle deformation will be further analyzed to define their relationships and
18 role in each deformational phase.

19

20 **6.1. Folds vs fracture patterns relationships**

21 The presence of gentle domes and basins with their longest axes oriented in orthogonal
22 directions (Section 3) suggests a regime of bi-directional compression ($\sigma_1 \sim \sigma_2 > \sigma_3$). Gosh
23 and Ramberg (1968) and Gosh et al. (1995) performed experimental investigations into the
24 development of domes and basins under constrictional deformation. The ~~Serra Geral Fm.~~ field
25 data recorded for São Bento Group upper formations do agree with experimental results in

1 that: i) domes and basins are elongated in orthogonal directions (Fig. 7A); ii) domes and
2 basins of the same deformational phase do not interfere with each other, but merge or abut
3 without crossing (Fig. 7A); and iii) the orthogonal fracture patterns and deformation bands are
4 set parallel and perpendicular to the elongated fold hinge (Fig. 15).

5 [Figure 15 summarizes the symmetry relationships between local and regional scale arcuate](#)
6 [folds and fractures \(joints and faults\). It includes field records and results \(Figs. 7–14\) for the](#)
7 [entire investigated area. These symmetry relationships support the development of fractures](#)
8 [as consequence of arcuate fold formation in a bi-directional stress state regime.](#)

9

10 **6.2. Stress/strain analysis for deformational phases**

11 A constrictional deformation regime is usually characterized by a stress difference ratio close
12 to 1 ($D = \Phi \sim 1$). It is common practice to evaluate the stress state from the stress ratio ($D =$
13 Φ ; Angelier, 1989) and Fig. 16A shows a histogram based on the results of the linear
14 inversion method (Gauss method; Žalohar and Vrabc, 2007). It can be seen that the D ratio
15 shows a wide dispersion for the first deformational phase, varying from 0.8 (area C), to 0.0–
16 0.3 in most of the studied sites.

17 The stress state for each deformational phase can also be evaluated on the diagram proposed
18 by Lisle (1979). This diagram (Fig. 16B) shows that the stress tensors for each site/area are
19 distributed in a linear pattern. This pattern suggests that the main stress difference ($\sigma_1 - \sigma_3$)
20 remains approximately constant, while σ_2 encompasses most of the variation. The N–S-
21 oriented stress field varies from a multidirectional stress field ($\sigma_1 > \sigma_2 \gg \sigma_3$), towards a
22 field where the major stress tensor is greater than the other two ($\sigma_1 \gg \sigma_2 \geq \sigma_3$). The NE–
23 SW-oriented stress field, however, is constrained to the field where the major compressive
24 tensor is greater than the other two.

1 The Morris and Ferril (2009) diagram analyzes the slip tendency of rock mass discontinuities
2 in terms of effective stress; i.e., the diagram can distinguish the influence of fluid pressure
3 (Fig. 16C). The first deformational phase (N–S paleostress) plots in two separate parallel lines
4 of constant slip tendency ($T_s = 1.3$ and 1.5). These two parallel lines suggest the varying
5 influence of the intermediate stress tensor (σ_2) on the deformation. However, the second
6 deformational phase (NE–SW paleostress) data correlate with a linear equation whose angular
7 coefficient is >-1.0 , which shows the influence of variations of both the σ_1 and σ_2 tensors on
8 the deformation.

9 The fault-slip data inversion also allows the strain condition of the deformational phases to be
10 evaluated (e.g., Marrett and Allmendinger, 1990; Cladouhos and Allmendinger, 1993;
11 Žalohar and Vrabec, 2008). Figure 17 shows the logarithmic diagram for strain ratio derived
12 from the Gauss Method (Žalohar and Vrabec, 2007), and from the MSM (Žalohar and
13 Vrabec, 2008). The MSM allows the strain ratio to be determined from the total displacement
14 gradient tensor of all measured fault sets, weighted by the number of faults in each set,
15 number of fault sets (their symmetry), and resolved shear stress (Žalohar and Vrabec, 2008).
16 The MSM strain values were defined by varying slightly the coefficient of residual friction
17 (ϕ_2) in the T-Tecto program. Such a procedure brought closer adjustment of the stress (Gauss)
18 and strain (MSM) tensors, because the axis of rotation is closer to a main tensor. Tables 5 and
19 6 show that the coefficients of residual friction (ϕ_2) determined from both the Gauss and
20 MSM inversion techniques are largely similar. The greatest difference in friction coefficient
21 ($7-10^\circ$) is related to those sites/areas with a small number of fault-slip data, or asymmetric
22 fault-slip sets.

23 Figure 17A represents the strain derived from the linear inversion technique and shows that
24 deformation was developed under constrictional conditions. This result is consistent with the
25 remote stress field, as discussed above. However, the strain ratio determined from the MSM

1 shows that both deformational phases could be distinguished based on this parameter, but
2 follow a flattening strain path (Fig. 17B). This flattening strain path results from a local stress
3 field, because most of the investigated sites [for fault-slip data inversion](#) represent a single
4 outcrop.
5 ~~However, it~~ must be noted, [on the other hand](#), that the flattening strain path (Fig. 17B) is
6 consistent in the volcanic rocks of the Paraná Basin, even for sites combining two or more
7 outcrops (see Žalohar and Vrabc, 2008). The highest ($\epsilon_2 - \epsilon_3$) MSM strain ratio is achieved
8 in those sites where conjugated faults or symmetric fault sets are best developed (see Fig. 13).
9 Additionally, the flattening strain path is best developed for the second deformational phase,
10 which could be a consequence of the higher degree of fractures inherited from the original
11 basalt flows and the first deformational phase.
12 The strain–ratio diagrams indicate a bi-directional constrictional deformation of the Paraná
13 Basin for both phases. However, a deformational model must be developed to account both
14 for the remote and local stress/strain fields and for the observed fracture patterns.

15

16 [6.3. Deformational model and the orientation of main horizontal stress tensors](#)

17 The deformational structures under investigation were developed upon [both upper formations](#)
18 [of the São Bento Group](#)~~the basalts to dacites of the Serra Geral Fm.~~ (Paraná Basin). The
19 volcanic flows [are dominantly massive](#), show large lateral extensions and are usually [more](#)
20 [than 20 m](#) thick (~~$\Rightarrow 20\text{ m}$~~)[\(Heemann, 1997, 2005; Reginato, 2003; Acauan, 2007; Amorim,](#)
21 [2007\)](#)~~; the main part of the basaltic flows are dominantly massive (Heemann, 1997, 2005;~~
22 ~~Reginato, 2003; Acauan, 2007; Amorim, 2007)~~. Thus, the buckling deformation must have
23 been produced by a tangential longitudinal mechanism (Ramsay, 1967, p. 391–415) and the
24 neutral surface must have played an important role in local strain partitioning and the
25 development of the [local scale](#) structures. Figure 18, based on the discussion by Lisle (1999),

1 summarizes a geometric model relating bi-directional constrictional domes and basins,
2 orthogonal fracture patterns, deformation bands, and conjugated faults.
3 The relations of symmetry of joints and faults to folds have long been investigated (e.g.,
4 Stearns, 1978; Hancock, 1985; Cosgrove and Ameen, 1999). The geometry of the domes and
5 basins in the Paraná Basin volcanics (Fig. 7) has to consider bi-directional constriction in
6 which both the major and intermediate ($\sigma_1 \geq \sigma_2$) remote tensors are horizontal. The buckling
7 mechanism operating simultaneously in the orthogonal direction gave rise to a local flattening
8 strain field in the outer part of the single flows, and open orthogonal extensional joints (Fig.
9 18). The fault-slip data, orthogonal joints, veins, and deformation bands were measured at the
10 outcrop scale and then developed to the outer buckled rim of each single volcanic flow of the
11 ~~Paraná Basin~~ Serra Geral Fm.

12 The elongation ratio and orientation of the greatest axis of the domes and basins (arcuate
13 folds) control stress/strain partition and orientation at this scale. Then, at domes and basins
14 scale, σ_{1db} orient parallel to the shortest axis, while σ_{2db} orient parallel to major axis. The local
15 flattening field in the outer rim of dome and basin, however, implies a third order stress/strain
16 partition ($\sigma_{1or} \gg \sigma_{2or} \geq \sigma_{3or}$). Both these conditions explain the main stress/strain tensor
17 permutation recorded in Figures 8 and 9 (Section 4): a) NS and EW (D_1), and ii) NW and NE
18 (D_2).

19 ~~Their~~ gentle interlimb angles of folds do not suggest large departures between the orientations
20 of the remote (upper order) and local tensors. Thus, even though the magnitudes and spatial
21 ~~distributions~~ position of the remote and local tensors differ, the extensional joints closely
22 parallel the main tensors and the axes of the domes and basins (cross bc and ac joints:
23 Hancock, 1985). This deformational model accounts for the square (Fig. 2F) or rectangular
24 (Fig. 12A) symmetry of the orthogonal veins, and for the “grid-type” deformation bands
25 (Figs. 12B and 14A).

1 The regional distribution of veins and dykes (Fig. 11) is in accordance with this deformation
2 history for the Paraná Basin ~~volcanics~~. The emplacement of the thermally metamorphosed
3 sandstone dykes could be attributed to the mobilization of the still unconsolidated sands from
4 the underlying Botucatu Fm., or from the Botucatu sands interlayered (intertrapped) between
5 the sequences of lava flows, into orthogonal extensional joints opened in the outer rim of the
6 buckled volcanic flows.

7 The shear fractures (hybrid joints and faults) display a conjugated arrangement with regard to
8 the extensional joints (Figs. 10, 11, 13), but they started to develop just after the orthogonal
9 fractures. The symmetry of the hybrid joints and faults is related to hk0 patterns in acute or
10 obtuse angles to the elongated fold axis (Hancock, 1985).

11

12 6.4. Local scale sStrike-slip stress regime and the stress drop

13 The strike-slip stress field determined from the fault-slip data (Sections 4 and 5) for both the
14 first and second deformational phases appears to be inconsistent with the local flattening
15 strain field in the outer part of the buckled volcanic flows. The fault-slip data showed that
16 rather than the major compressive tensor being vertical (σ_{1or}), it was the local intermediate
17 ~~compressive~~ tensor (σ_{2or}) instead. However, the onset extensional joints induce local stress
18 release in the σ_{1or} direction and a permutation between the local σ_{1or} and σ_{2or} tensors. This
19 stress drop explains why the main stress difference ($\sigma_1 - \sigma_3$) remains approximately constant
20 (Fig. 16).

21 The stress/strain main tensor positioning after local stress release ($\sigma_{1sd} > \sigma_{2sd} > \sigma_{3sd}$,
22 intermediate tensor now in vertical position) characterize the strike-slip stress state, and
23 generates-controls strike-slip faults (hk0 fault symmetry pattern) in the Jurassic to Cretaceous
24 formations of the Paraná Basin. These deformational conditions explain the connection of
25 extensional joints and hybrid to shear fractures, as shown in Figs. 2 and 11A.

1 The bi-directional constrictional deformation in the Paraná Basin during the Jurassic to
2 Cretaceous periods, then, accounts for the outcrop-scale alternation of σ_3 (σ_{3sd}) position, i.e.,
3 either N–S or E–W in the first deformational phase, or NE or NW in the second deformational
4 phase. ~~In fact, the different σ_1 and σ_3 orientations distinguished in Figs. 8 and 9 are not related~~
5 ~~to local σ_1 and σ_2 permutations on the outer rims of the folded volcanic flows.~~ It should be
6 noted that σ_1 (σ_{1sd}) and σ_3 (σ_{3sd}) orientations alternate between different investigation sites.
7 Thus, it can be concluded that σ_1 (σ_{1sd}) and σ_3 (σ_{3sd}) orientations, inverted from fault-slip data,
8 are related to the elongation of the dome-and-basin structures developed in each area. ~~The bi-~~
9 ~~directional constrictional ($\sigma_1 \geq \sigma_2 \gg \sigma_3$) stress regime gave rise to orthogonally oriented~~
10 ~~domes and basins, as shown by Gosh and Ramberg (1968) and Gosh et al. (1995), which~~
11 ~~controlled the local distribution of extensional joints and strike-slip faults.~~

12 These deformational conditions explain the connection between extensional joints and hybrid
13 to shear fractures, as shown in Figs. 2 and 11A. The extensional joints and their splays to
14 hybrid and shear fractures frequently have hydraulic breccia (Fig. 2). Such a feature points to
15 supra-hydrostatic conditions ($P_f/P_{grav} > 0.4$) during the deformation, which favor the
16 development of extensional joints. Veins and associated hydraulic breccia are also developed
17 on fractures related to the second deformational phase, i.e., the supra-hydrostatic conditions
18 remained active during this deformational phase.

19 This structural model of the constrictional deformation in the Paraná Basin also accounts for
20 other important features observed in the volcanic flows. Small-scale folds, similar to that in
21 Fig. 7E, are recorded on basal horizontally jointed portions of the volcanic flows (Fig. 19).
22 These small-scale folds are frequently truncated by fracture zones at their limbs. These folds,
23 however, are developed in the inner zone of the dome-and-basin structures, which is the locus
24 for the local constrictional stress/strain in the tangential–longitudinal mechanism (Fig. 19C).
25 Thus, it can be concluded that buckling of a single lava flow gave rise to the distinguishing

1 deformational structures on either side of its neutral surface. At the outer rims, orthogonal
2 extensional joints developed and sandstones dykes were emplaced, while at the inner rims,
3 non-cylindrical folds developed.

4 5 6.5. Time constrain to deformation

6 The fault-slip and structural data for this investigation derive from the Botucatu and Serra
7 Geral formations (upper units of São Bento Group) of the Paraná Basin~~The deformational~~
8 ~~structures of the volcanic rocks of the Serra Geral Fm. were developed during the Jurassic to~~
9 ~~Cretaceous periods.~~ Lava flow stratigraphy differs in each of the studied sites/areas
10 (Heemann, 1997, 2005; Reginato, 2003; Acauan, 2007; Amorim, 2007), and it is still not
11 possible to correlate the studied quarries to specified time intervals taking into account
12 stratigraphic elements. However the investigated structural elements (folds, joints and faults)
13 can be time constrained based in some regional features. This time intervals will certainly be
14 refined in future detailed investigation.~~, the fault slip investigations were constrained to the~~
15 ~~Serra Geral Fm. volcanics and intertrap sediments, which left the exact time of onset of the~~
16 ~~first deformational phase to be defined~~

17 The onset of the first deformational episode, however, is not constrained by the volcanic
18 flows and underlying Botucatu Fm. The analysis of the thickness distribution for the
19 underlying Meso-triassic sequence (Artur and Soares, 2002), and also for the Pirambóia–
20 Guará and Botucatu formations (lower units of São Bento Group, Soares et al., 2008b) shows
21 a series of N–S elongated and circular structures. These results suggests that the stress field
22 for the first deformational episode might have operated from at least the Triassic (lower
23 bound) to the Early Jurassic period (upper bound) onwards.

24 For structural purposes, geochronological data produced in association with palaeomagnetic
25 studies for volcanic rocks related to the Paraná Basin can improve structural analysis, because

1 it introduces better differentiation between the relative timings of volcanic structures (flows,
2 dykes, and sills).

3 Palaeomagnetic data and precise absolute ages for Mesozoic basic rocks related to the Serra
4 Geral Fm. volcanism clearly distinguish three groups (see Ernesto, 2006,2009, for a revision):
5 a) Serra Geral flows, b) Ponta Grossa Arc and Serra do Mar basic dyke swarms, and c)
6 Florianópolis Dyke Swarm. While some overlap of apparent ages and virtual geomagnetic
7 poles (VGPs) exists, it should be noted that the Serra Geral flows are older (time span 135–
8 132 Ma) and show VGPs oriented to 83/090. The Ponta Grossa Dyke Swarm (PGDS) shows
9 ages spanning from 132–129 Ma and has a mean VGP directed towards 82/059. The
10 Florianópolis dykes have a time span in the interval 127–121 Ma and a VGP oriented to
11 88/003.

12 Ponta Grossa Arc and its Dyke Swarm (PGDS) are one of the main structural feature of the
13 Paraná Basin (Fig. 5). The mean axial planes (305/84) and arc axes (06/307) of these
14 structures are all compatible with a mean compressive stress field directed to 035–040 (D2
15 deformational phase). The mean direction for the basic dykes of the Ponta Grossa Arc is 300–
16 310 (e.g., Strugale et al., 2007). These structural relationships indicate that the PGDS was
17 emplaced in extensional fractures developed at the outer hinge zone in an anticlinal fold (Fig.
18 6) including Paraná Basin basement. The PGDS crosscut the basement rocks, and sedimentary
19 and volcanic rocks of the Paraná Basin (e.g., Strugale et al., 2007). In this scenario, the PGDS
20 cannot be regarded as an aborted rift arm, as it has previously been interpreted (e.g., Morgan,
21 1971; Chang et al., 1992; Turner et al., 1994).

22 The emplacement of the Ponta Grossa dykes (PGDS), then, can be taken as the upper age
23 limit for the onset of the second deformational episode (ca. 132 Ma). And, thus, the first (D1)
24 deformational phase can be constrained, in a first approximation, to ca. 200–132 Ma interval.

1 An upper age limit to D2 deformation can be taken from the emplacement of the
2 Florianópolis dykes. Raposo et al. (1998) related them to extension of the South America
3 crust just prior to the Atlantic oceanic crust expansion. Thus, the second (D2) deformational
4 phase can be preliminary constrained to ca. 132–121 Ma interval.

6 **7. Conclusions**

7 The geometric, ~~and~~ kinematic and dynamic analyses of ~~the~~ field data permitted to characterize
8 a regional bi-directional constrictional ($\sigma_1 \geq \sigma_2 \gg \sigma_3$) stress state regime ~~two deformational~~
9 ~~phases~~ during the Jurassic to Cretaceous periods ~~to be distinguished~~ of the Paraná Basin. Two
10 ~~Both~~ deformational phases were developed under these regional ~~bi-directional~~ constrictional
11 ~~($\sigma_1 \geq \sigma_2 \gg \sigma_3$)~~ stress regimes and gave rise to a number of non-cylindrical folds. These
12 structures are characterized as domes and basins, and regional anticlines and synclines.
13 Consequently, both deformational phases produced similar local-scale structures, that .
14 ~~However, these deformational phases~~ can be distinguished both by the orientation ~~of their~~
15 ~~structures~~ and by some ~~other~~ particular structural features. The first deformational phase
16 shows elongated domes and basins oriented both N–S and E–W. The second deformational
17 phase also shows elongated domes and basins, but these are oriented NW–SE and NE–SW,
18 according to the most expressive Ponta Grossa and Rio Grande arcs, and the Torres Syncline
19 in the eastern border region of the Paraná Basin. These conditions indicate a clockwise
20 rotation (35–40°) for both horizontal principal stress tensors ($\sigma_1 \geq \sigma_2$) during the Cretaceous
21 period.

22 The stress/strain partition at different scales was responsible for structural features recorded at
23 decreasing scales in the Paraná Basin. The orthogonal orientation of the major axis of domes
24 and basins controls alternated orientation of stress/strain tensors ($\sigma_{1db} \geq \sigma_{2db}$) at this scale.

1 The tangential longitudinal buckling mechanism supported by massive, thick volcanic layers
2 enabled local scale stress/strain partition between outer and inner arcuate folds. The outer rim
3 developed orthogonal patterns of the dykes and veins, and also deformation bands, retaining
4 symmetric relationships with the fold axes of the elongated domes and basins. The inner rims
5 of the buckled volcanic flows, however, developed local arcuate folds, whose local stress axes
6 are close to the regional ones. It should be noted that local-scale folds could reproduce the
7 regional bi-directional constrictional regime. ~~Further investigations are needed to address this~~
8 ~~point in the future.~~

9 ~~These orthogonal extensional joints are developed in the outer rims of the folded volcanic~~
10 ~~flows; however, the strike-slip faults follow the development of extensional joints. The strike-~~
11 ~~slip faults are the result of the stress drop after the onset of the extensional joints, which~~
12 ~~enabled a local permutation between σ_1 and σ_2 . The hk0 symmetry for the strike-slip faults in~~
13 ~~the arcuate folds is in accordance with field observations.~~

14 The stress/strain condition in the outer rim of arcuate folds (flattening) governs ~~outerop-scale~~
15 ~~alternation of the σ_{3sd} position, either N-S or E-W (D1 phase), or NE or NW (D2 phase), is~~
16 ~~not related to~~ after stress drop due to extensional fractures onset. These conditions are
17 supported by the fact that ~~The different σ_1 and σ_3 orientations distinguished in Figs. 8 and 9~~
18 ~~are mainly reported in different investigation sites and result from the orientation of the~~
19 ~~arcuate fold minor axis. Thus, the σ_3 position depends on the orientation of the orthogonal~~
20 ~~elongated domes and basins. Thus, further investigation is in progress to determine the~~
21 ~~regional (remote), rather than local stress/strain field in the Jurassic to Cretaceous periods of~~
22 ~~the Paraná Basin.~~

23 ~~These orthogonal extensional joints are developed in the outer rims of the folded volcanic~~
24 ~~flows; however, the~~ strike-slip faults follow the development of extensional joints. The strike-
25 slip faults are, then, the result of the stress drop after the onset of the extensional joints, which

1 enabled a local scale permutation between σ_{1or} and σ_{2or} . ~~The hk0 symmetry for the strike-slip~~
2 ~~faults in the arcuate folds is in accordance with field observations.~~

3 ~~The paleostress inversion based distinction of fracture orientation families introduces biased~~
4 ~~results in some previous papers. The field-based data (fault slips, fracture patterns, dykes, and~~
5 ~~contact attitudes) and data derived from paleostress inversions and kinematic analyses are in~~
6 ~~agreement with each of the deformational phases.~~

7 The paleostress orientation derived from fault-slip data, ~~however~~thus, is related to the local
8 stress field developed upon the buckled single volcanic flows of the Serra Geral Fm. after
9 stress drop episodes.

10 ~~The se general orientations for the NE-SW (NW-SE) stress tensors agree with those~~
11 ~~presented strike-slip stress state regime proposed by Riccomini (1995), Strugale et al. (2007),~~
12 ~~Machado et al. (2012), and Nummer et al. (2014), then, is a local scale stress field. Thies~~
13 ~~strike-slip stress state regime differ, however, was applied on specific way for data~~
14 ~~processing methodology and kinematic analysis by those authors. Then, the deformational~~
15 ~~phases discriminated It should be noted that the area studied by Riccomini (1995), and~~
16 ~~Strugale et al. (2007), Machado et al. (2012), and Nummer et al. (2014) are hard is heavily~~
17 ~~influenced by the NW-SE Ponta Grossa faults and dikes. Despite final results that are~~
18 ~~difficult to reconcile with results obtained in this study without introducing biased~~
19 ~~interpretation, it seems that the D1 faults (deformation) defined by Strugale et al. (2007)~~
20 ~~correspond to the D2 deformational phase discussed here.~~

21 ~~The Gauss and MSM paleostress inversion methods (Žalohar and Vrabc, 2007, 2008) were~~
22 ~~applied to fault slip data for 42 sites in the southeast border and central regions of the Paraná~~
23 ~~Basin (Brazil). A number of fieldwork campaigns were undertaken to map the important~~
24 ~~structural features of the Paraná Basin that developed during the Jurassic to Cretaceous~~
25 ~~periods.~~

1
2
3
4
5
6
7
8
9
10
11
12
13
14
15
16
17
18
19
20
21
22
23

Author contribution

A.J.S, R.H., P.A.R.R., R.B.A., V.A.A., and M.Z.R participated in the study design and concept, data collection, and data analysis and interpretation during the first stages of the investigation. A.J.S. also supervised all the investigation and conducted the second stage of field work, data analysis and interpretation. A.J.S. wrote the main manuscript, and R.H., P.A.R.R., R.B.A., V.A.A., and M.Z.R conducted critical review and suggested amendments to the final manuscript.

Acknowledgments

The authors especially thank Dr. Jure Žalohar for kindly providing a license for the T-Tecto 3.0 software (http://www2.arnes.si/~jzaloh/t-tecto_homepage.htm), and for reading the article and offering comments and suggestions for its improvement. The authors also thank Dr. Luis Eduardo S.M. Novaes and Dr. Bardo Bodmann for their comments regarding this work.

Authors would also thank to Topical Editor (Dr. Federico Rossetti) and the Referees. Special thanks to the Referee 1 for their careful consideration and comments that have helped us improve the quality of the article.

The authors thank the Brazilian research agencies (FAPERGS, CNPq, CAPES, FINEP) for supporting the initial projects regarding the Paraná Basin volcanic rocks, and the Universidade Federal de Pelotas for supporting and encouraging the more recent local and regional fieldwork campaigns.

1
2
3
4
5
6
7
8
9
10
11
12
13
14
15
16
17
18
19
20
21
22
23
24
25
26

References

Aboy, M., and Masquellin, H.: Relações embasamento vs. cobertura na Ilha Cristalina de Rivera, Uruguai, in: Simpósio Sul-brasileiro de Geologia, Abstracts, SBG, Porto Alegre (Brazil), 126, 2013.

Acauan, R. B.: Geologia e controle estrutural das ocorrências de ágatas e ametistas na região de Quaraí/Santana do Livramento (RS). Master degree Dissertation, PrPG em Engenharia de Minas, Metalurgia e Materiais, UFRGS, Brazil, 167 pp., 2007.

Almeida, F. F. M.: Síntese sobre a tectônica da Bacia do Paraná, in: Simp. Regional de Geologia, 3, SBG-SP, Curitiba (Brazil), 1, 1–20, 1981.

Amorim, V. A.: Modelagem geológica e controle dos depósitos em geodos no Distrito Mineiro de Ametista do Sul (RS, Brasil). Master degree Dissertation, PrPG em Engenharia de Minas, Metalurgia e Materiais, UFRGS, Brazil, 173 pp., 2007.

Angelier, J.: From orientation to magnitudes in paleostress determinations using fault slip data. *J. Struct. Geol.*, 11, 37–50, 1989.

Angelier, A. and Mechler, P.: Sur une méthode graphique de recherche de contraintes principales également utilisable et en séismologie: la méthode des diédres droits. *Bull. Soc. Geol. Fr.*, 19, 1309–1318, 1977.

Artur, P. C. and Soares, P. C.: Paleoestruturas e petróleo na bacia do Paraná, Brasil. *Revista Brasileira de Geociências*, 32, 433–448, 2002.

Bai, T., Maerten, L., Gross, M. R. and Aydin, A.: Orthogonal cross joints: do they imply a regional stress rotation? *J. Struct. Geol.*, 24, 77–88, 2002.

Caputo, R.: Evolution of orthogonal sets of coeval extension joints. *Terra Nova*, 7, 479–490, 1995.

Caputo, R. and Hancock, P. L.: Crack-jump mechanism and its implications for stress cyclicity during extension fracturing. *J. Geodyn.*, 16, 34–59, 1999.

- 1 Chang, H. K., Kowsmann, R. O., Figueiredo, A. M. F. and Bender, A. A.: Tectonics and
2 stratigraphy of the East Brazil rift system: an overview. *Tectonophysics*, 213, 97–138,
3 1992.
- 4 Cladouhos, T. T. and Allmendinger, R. W.: Finite strain and rotation from fault-slip data. *J.*
5 *Struct. Geol.*, 15, 771–784, 1993.
- 6 Cosgrove, J. W. and Ameen, M. S.: A comparison of the geometry, spatial organization and
7 fracture patterns associated with forced folds and buckled folds. *Geol. Soc. Spec.*
8 *Publ.*, 169, 7–22, 1999.
- 9 [Ernesto, M.: Drift of South American Plate since Early Cretaceous: reviewing the Apparent](#)
10 [Polar Wander path. *Geociências*, 25, 83–90, 2006.](#)
- 11 [Ernesto, M.: Contribuições dos estudos paleomagnéticos ao entendimento da abertura do](#)
12 [Atlântico. *Boletim de Geociências da PETROBRAS*, 17, 353–363, 2009.](#)
- 13 Ferreira, F. J. F.: Integração de Dados Geofísicos e Geológicos: Configuração e Evolução
14 Tectônica do Arco de Ponta Grossa. Dissertação de Mestrado, PPG em Geoquímica e
15 Geotectônica, IG-USP, São Paulo (Brasil), 273 pp., 1982.
- 16 Ferreira, F. J. F.; Monma, R.; Campanha, G. A. C. and Galli, V. L.: Na estimate of the degree
17 of crustal extension and thinning associated with the Guapiara Lineament based on
18 aeromagnetic modelling. *Boletim IG-USP, Série Científica*, 20, 69–70, 1989.
- 19 Gosh, S. K. and Ramberg, H.: Buckling experiments on intersecting fold patterns.
20 *Tectonophysics*, 5, 89–105, 1968.
- 21 Gosh, S. K., Khan, D. and Sengupta, S.: Interfering folds in constrictional deformation. *J.*
22 *Struct. Geol.*, 17, 1361–1373, 1995.
- 23 Hancock, P. L.: Brittle microtectonics: principles and practice. *J. Struct. Geol.*, 7, 437–457,
24 1985.

- 1 Heemann, R.: Geologia, controles e guias prospectivos dos depósitos de ágata na região de
2 Salto do Jacuí (RS). Master degree Dissertation, PrPG em Engenharia de Minas,
3 Metalurgia e Materiais, UFRGS, Brazil, 107 pp., 1997.
- 4 Heemann, R.: Modelagem exploratória estrutural e tridimensional para a prospecção dos
5 depósitos de ágata do Distrito Mineiro de Salto do Jacuí (RS). PhD thesis, PrPG em
6 Engenharia de Minas, Metalurgia e Materiais, UFRGS, Brazil, 163 pp., 2005.
- 7 Jacques, P. D.; Machado, R.; Oliveira, R. G.; Ferreira, F. J. F.; Castro, L. G. and Nummer, A.
8 R.: Correlation of lineaments (magnetic and topographic) and Phanerozoic brittle
9 structures with Precambrian shear zones from the basement of the Paraná Basin, Santa
10 Catarina State, Brazil. *Bra J Geol*, 44, 39–54, 2014.
- 11 Jaeger, J. C.: *Elasticity, Fracture and Flow: with Engineering and Geological Applications*.
12 Chapman & Hall, London, 268 pp., 1969.
- 13 Leinz, V., Bartorelli, A. and Isotta, C. A. L.: Contribuição ao estudo do magmatismo basáltico
14 Mesozóico da Bacia do Paraná. *Academia Brasileira de Ciências*, 40, 167–181, 1968.
- 15 Lisboa, N. A. and Schuck, M. T. G. O.: Identificação de padrões estruturais no Grupo São
16 Bento, Quaraí, RS, através de imagens orbitais e sub-orbitais. *Pesquisas em*
17 *Geociências*, 20, 5–23, 1987.
- 18 Lisle, R. J.: The representation and calculation of the deviatoric component of the geological
19 stress tensor. *J. Struct. Geol.*, 1, 317–321, 1979.
- 20 Lisle, R. J.: Predicting patterns of strain from three-dimensional fold geometries: neutral
21 surface folds and forced folds. *Geol. Soc. Spec. Publ.*, 169, 213–221, 1999.
- 22 Machado, R.; Roldan, L. F.; Jacques, P. D.; Fassbinder, E. and Nummer, A. R.: Tectônica
23 transcorrente Mesozoica-cenozóica no Domo de Lages – Santa Catarina. *Revista*
24 *Brasileira de Geociências*, 42, 799–811, 2012.

- 1 Marrett, R. and Allmendinger, R. W.: Kinematic analysis of fault-slip data. *J. Struct. Geol.*, 12
2 973–986, 1990.
- 3 Marshak, S. and Mitra, G.: Basic methods of structural geology. Prentice Hall, New Jersey
4 (USA), 446 pp., 1988.
- 5 Meirelles, M. C.: Determinação da resistência ao cisalhamento de enrocamentos da UHE
6 Machadinho através de ensaios de cisalhamento direto de grandes dimensões. Master
7 degree Dissertation, PrPG Engenharia Civil, UFSC, Brazil, 123 pp., 2008.
- 8 [Morgan, W. J.: Convection plumes in the lower mantle. *Nature*, 230, 42–43, 1971.](#)
- 9 Morgan, W. J.: Hotspot tracks and the early rifting of the Atlantic. *Tectonophysics*, 94, 123–
10 139, 1983.
- 11 Morris, A. P. and Ferrill, D. A.: The importance of the effective intermediate principal stress
12 (σ_2) to fault slip patterns. *J. Struct. Geol.*, 31, 950–959, 2009.
- 13 Northfleet, A. A., Medeiros, R. A. and Mühlmann, H.: Reavaliação dos dados geológicos da
14 Bacia do Paraná. *Boletim Técnico da PETROBRAS*, Rio de Janeiro, 12, 291–346,
15 1969.
- 16 Nummer, A. R., Machado, R. and Jacques, P. D.: Tectônica transcorrente
17 mesozoica/cenozoica na porção leste do Planalto do Rio Grande do Sul, Brasil.
18 *Pesquisas em Geociências*, 41, 121–130, 2014.
- 19 Petit, J. P.: Criteria for the sense of movement on fault surfaces in brittle rocks. *J. Struct.*
20 *Geol.*, 9, 597–608, 1987.
- 21 Quintas, M. C. L.: O embasamento da Bacia do Paraná: reconstrução geofísica de seu
22 arcabouço. Tese de Doutorado, PPG em Geofísica (IAG-USP), São Paulo (SP),
23 213 pp., 1995.
- 24 Ramsay, J.: Folding and fracturing of rocks. McGraw-Hill, New York, 568 pp., 1967.

- 1 [Raposo, M. I. B., Ernesto, M., and Renne, P. R.: Paleomagnetism and \$^{40}\text{Ar}/^{39}\text{Ar}\$ dating of the](#)
2 [Early Cretaceous Florianópolis dike swarm \(Santa Catarina Island\), Southern Brazil.](#)
3 [Earth and Planetary Science Letters, 108, 275–290, 1998.](#)
- 4 Reginato, P. A. R.: Integração de dados geológicos para prospecção de aquíferos fraturados
5 em trecho da Bacia Hidrográfica Taquari-Antas (RS). PhD thesis, PrPG em
6 Engenharia de Minas, Metalurgia e Materiais, UFRGS, Brazil, 286 pp., 2003
- 7 Reginato, P. A. R and Strieder, A. J.: Caracterização estrutural dos aquíferos fraturados da
8 Formação Serra Geral na região nordeste do Estado do Rio Grande do Sul. Revista
9 Brasileira de Geociências, 36, 13–22, 2006.
- 10 Remde, M. Z.: A megaduna intertrap do Cerro do Jarau (RS). Bachelor degree Dissertation,
11 Engenharia Geológica, CDTEC-UFPel, 95 pp., 2013.
- 12 Riccomini, C.: Tectonismo gerador e deformador dos depósitos sedimentares pós-
13 gondvânicos da porção centro-oriental do Estado de São Paulo e áreas vizinhas. Tese
14 de Livre Docência, Instituto de Geociências, Universidade de São Paulo, São Paulo
15 (Brasil), 100 pp., 1995.
- 16 Rives, T., Rawnsley, K. D. and Petit, J. P.: Analogue simulation of natural orthogonal joint set
17 formation in brittle varnish. J. Struct. Geol., 16, 419–429, 1994.
- 18 Rostirolla, S. P., Assine, M. L., Fernandes, L. A. and Artur, P. C.: Reativação de
19 Paleolineamentos durante a evolução da Bacia do Paraná - O Exemplo do Domo de
20 Quatiguá. Revista Brasileira de Geociências, 30, 639–648, 2000.
- 21 Scherer, C. M. S. and Lavina, E. L. C.: Stratigraphic evolution of fluvial-eolian succession: the
22 example of the Upper Jurassic-Lower Cretaceous Guarú and Botucatu formations,
23 Paraná Basin, Southern Brazil. Gondwana Res., 9, 475–484, 2006.
- 24 Schobbenhaus, C. and Bellizzia, A.: Geological Map of South America. 1:5.000.000 CGMW
25 – CPRM – DNPM – UNESCO, Brasília (Brazil), 2001.

- 1 Schuck, M. T. G. O. and Lisboa, N. A.: Caracterização de formas e padrões estruturais no
2 Grupo São Bento da Bacia do Paraná no Rio Grande do Sul em imagens orbitais e sub-
3 orbitais. *In: Simpósio Brasileiro de Sensoriamento Remoto*, 1988, Natal (Brazil),
4 *Anais*, 2, 323–333, 1988.
- 5 Soares, A. P., Barcellos P. E., Csordas S. M., Mattos, J. T., Balieiro, M. G. and Meneses, P.
6 R. Lineamentos em imagens de Landsat e Radar e suas implicações no conhecimento
7 tectônico da Bacia do Paraná, in: *Simp. Bras. Sens. Remoto*, 2, Brasília, 143–168,
8 1982.
- 9 Soares, A. P., Soares, P. C. and Holz, M.: Correlações conflitantes no limite Permo-Triássico
10 no sul da Bacia do Paraná: o contato entre duas superseqüências e implicações na
11 configuração espacial do Aquífero Guarani. *Pesquisas em Geociências*, 35, 115–133,
12 2008a.
- 13 Soares, A. P., Soares, P. C. and Holz, M.: Heterogeneidades hidroestratigráficas no Sistema
14 Aquífero Guarani. *Revista Brasileira de Geociências*, 38, 598–617, 2008b.
- 15 Stearns, D. W.: Faulting and forced folding in the Rocky Mountain foreland. *Geol. Soc. Am.*
16 *Mem.*, 151, 1–38, 1978.
- 17 Strieder, A. J. and Heemann, R.: Análise geométrica de estruturas de sucessão vulcânica
18 associada aos depósitos de Ágata do Distrito Mineiro do Salto do Jacuí (RS), in:
19 *Simpósio Nacional de Estudos Tectônicos, Extended Abstracts*, 1, Lençóis (BA), 14–
20 16, 1999.
- 21 Strugale, M., Rostirolla, S. P., Mancini, F., Portela Filho, C. V., Ferreira, F. J. F. and Freitas,
22 R. C.: Structural framework and Mesozoic–Cenozoic evolution of Ponta Grossa Arch,
23 Paraná Basin, southern Brazil. *J. S. Am. Earth Sci.*, 24, 203–227, 2007.
- 24 Tchalenko, J. S.: Similarities between shear zones of different magnitudes. *Geol. Soc. Am.*
25 *Bull.*, 81, 1625–1640, 1970.

- 1 Tchalenko, J. S. and Ambraseys, N. N.: Structural analysis of the Dasht-e Bayaz (Iran)
2 earthquake fractures. *Bull. Geol. Soc. Am.*, 81, 41–60, 1970.
- 3 [Turner, F. J. and Weiss, L. E.: Structural analyses of metamorphic tectonites. McGraw-Hill
4 Book Company Inc., New York \(USA\), 536 pp., 1963](#)
- 5 [Turner, S., Regelous, M., Kelley, S., Hawkesworth, C., and Mantovani, M.: Magmatism and
6 continental break-up in the South Atlantic: high precision ⁴⁰Ar-³⁹Ar geochronology.
7 *Earth Planetary Science Letters*, 121, 333–348, 1994.](#)
- 8 Wilson, M.: *Igneous petrogenesis: a global tectonic approach*. Chapman & Hall Ed., London
9 (UK), 466 pp., 1989
- 10 Zalán, P. V.: Evolução Fanerozóica das bacias sedimentares brasileiras, in: Neto, V.M.,
11 Bartorelli, A., Carneiro, C.d.R. and Brito-Neves, B.B., *A Geologia do Continente Sul-
12 americano*, Editora Beca, São Paulo (Brazil), 595–613, 2004.
- 13 Zalán, P. V., Wolff, S., Astolfi, M. A. M., Vieira, I. S., Conceição, J. C. J., Appi, V. T., Neto,
14 E. V. S., Cerqueira, J. R. and Marques, A.: The Paraná Basin, Brazil. *AAPG Memoir.*,
15 51, 681–707, 1991.
- 16 Žalohar, J. and Vrabec, M.: Paleostress analysis of heterogeneous fault-slip data: the Gauss
17 method. *J. Struct. Geol.*, 29, 1798–1810, 2007.
- 18 Žalohar, J. and Vrabec, M.: Combined kinematic and paleostress analysis of fault-slip data:
19 the multiple-slip method. *J. Struct. Geol.*, 30, 1603–1613, 2008.
- 20 Zerfass, H., Chemale Jr, F. and Lavina, E. L. C.: Tectonic control of the Triassic Santa Maria
21 Supersequence of the Paraná Basin, Southernmost Brazil, and its correlation to the
22 Waterberg Basin, Namibia. *Gondwana Res.*, 8, 163–176, 2005.
- 23
24

1 Table 1 Deformational phases distinguished in the uppermost units of the Paraná and in the
 2 continental rift basins of Southeast Brazil (Riccomini 1995)

Def Phase	Time interval	Main geological features	Interpretation
D _n	Permian to Lower Cretaceous	Deformational event previous to Gondwana rupture NE-oriented basalt and clastic dikes Geophysical alignments	NW-oriented minimum stress (σ_3) axis
D _{n+1}	Upper Cretaceous	NW-oriented basalt dikes in the Ponta Grossa Arc region Final stages of the Serra Geral volcanism Jacupiranga Alkaline Intrusion Anticlinal dome structures	<i>NE basalt dikes and NW Ponta Grossa dikes were indicated to represent a triple junction remnant</i> NE-oriented minimum stress (σ_3) axis Dextral transcurrent system
D _{n+2}	Paleocene to Eocene	Bauru Basin structural development Rift (graben) basins at the continental margin NE-oriented lamprophyric dikes	NW-oriented minimum stress (σ_3) axis Sinistral transcurrent system
D _{n+3}	Eocene to Oligocene	Jaboticabal Alkaline Intrusion Hydrothermal silicification contemporaneous to sedimentation of Itaqueri Fm.	NNW-oriented maximum stress (σ_1) axis Dextral transcurrent system
D _{n+4}	Miocene	Ultrabasic flows in Volta Redonda and Itaboraí Deposition of Itaquaquecetuba Fm.	Sinistral EW transcurrent system Maximum stress (σ_1) axis alternating from NS and EW according the balance between South Atlantic drifting and Nazca Plate subduction
D _{n+5}	Pliocene		
D _{n+6}	Pleistocene to Holocene	NS-oriented grabens Extensional WNW-ESE regime	

3

4

1 Table 2 Paleostress fields defined by Heemann (1997, 2005), Reginato (2003), Acauan (2007)
 2 and Amorim (2007) for fault slip data of Serra Geral Fm using the method of Angelier and
 3 Mechler (1977). [Structural elements notation in this paper follows the Right Hand Rule](#)
 4 [\(RHR\)](#).

	(σ_1)	(σ_2)	(σ_3)
Heemann (1997,2005), Heemann and Strieder (1999)			
Salto do Jacuí and Sobradinho region (RS)			
Estrela Velha – Arroio do Tigre área	20-341	35-100	08-219
Sobradinho to Ibarama área	11-321	67-182	02-095
Saltinho área	06-334	72-218	02-120
	12-151	50-044	34-260
Eng. Maia Filho Damp area	04-343	30-250	58-095
	46-357	22-110	13-209
Angico Quarry	36-349	05-255	52-157
Poço Grande Quarry	19-358	14-091	12-178
Zubi and Ralph Quarries	67-341	04-079	23-172
	62-313	15-073	06-165
Pedreira Funda Quarry	50-332	07-086	05-171
Reginato (2003), Reginato and Strieder (2006)			
Caxias do Sul and Veranópolis region (RS)			
Pedreira Guerra Quarry	10-074	80-256	03-346
CODECA Quarry	01-174	86-084	04-264
	03-263	88-092	02-357
Tega Outcrop and Road cut	15-073	72-270	04-165
Veranópolis roadcut	10-068	80-248	02-158
Acauan (2007)			
Santana do Livramento and Quaraí region (RS)			
Santa Rita Quarry	11-032	87-182	07-301
	08-133	80-272	07-042
Registro Quarry	09-116	80-270	04-026
Amorim (2007)			
Ametista do Sul and Frederico Westphalen region (RS)			
Ametista do Sul quarries	25-028	54-330	23- 115
Frederico Westph to Caiçara area	13-110	68-327	17-204
	09-170	72-328	17-083
	20-205	60-334	21-114
Rodeio Bonito Quarry	09-147	70-355	18-241
	29-232	54-355	21-139

1 Table 3 Summary of crosscutting relations of different striations observed in the same fault
2 plane

Site	Relative age	Fault plane	Striae orientation	Sense of movement
Pedreira Quarai	1 st	359/73	20/173	Sinistral
	2 nd	359/73	14/006	Dextral
Pedreira SF Assis	1 st	066/72	27/236	Dextral
	2 nd	066/72	27/077	Sinistral
Pedreira Painei	1 st	166/72	09/343	Dextral
	2 nd	166/72	10/169	Dextral
	1 st	034/74	13/039	Sinistral
	2 nd	034/74	60/185	Normal

3

4

1 Table 4 Parameters for stress inversion using multiple-slip method (Žalohar and Vrabec
2 2008).

Parameter	Value range
Dispersion (s)	20
Threshold (Δ)	40–50
Shear strength (ϕ_1)	50–65
Angle of residual friction (ϕ_2)	20–35
Stress parameter	40–50
Andersonian regime set	Yes

3 The shear strength and angle of internal friction data for volcanic rocks of Paraná Basin are
4 from fresh rock test (Meirelles 2008).

5

6 Table 5 Summary of principal stress axes in the N–S and E–W orientations computed for sites within the volcanic rocks of the Paraná Basin.

Site	Standard deviation of s	Linear inversion							MSM inversion							
		σ_1	σ_2	σ_3	Relative values of λ_i			D	ϕ_2	σ_1	σ_2	σ_3	Relative values of λ_i		D	ϕ_2
A Compilation from PR (Ped Registro) and PQ2 (Ped Quaraí 2)	13	02/260	84/009	06/170	0.56 : -0.24 : -0.33			0.10	25	01/264	87/011	03/174	0.73 : -0.03 : -0.70		0.47	20
B Pedreira SF Assis 2 (BR377)	20	02/273	72/176	18/003	0.58 : -0.24 : -0.34			0.10	25	12/275	78/104	02/006	0.71 : 0.03 : -0.73		0.53	25
C Compilation from sites Estr Velha, Sobradinho1, and Saltinho1A	14	02/174	84/283	06/084	0.24 : 0.12 : -0.36			0.80	35	08/174	78/305	09/082	0.71 : 0.03 : -0.74		0.53	20
D Compilation from sites Angico and Poço Grande	17	12/184	76/030	06/275	0.48 : -0.11 : -0.37			0.30	35	01/190	83/094	07/280	0.73 : -0.01 : -0.73		0.49	35
E Compilation from sites Sobradinho2, Saltinho2, Gar Zubi, and Pedra Funda	17	02/260	84/152	06/350	0.52 : -0.17 : -0.35			0.20	30	03/086	87/239	01/356	0.71 : 0.01 : -0.71		0.51	30
F Compilation from sites Gar Ametista, Pedr Fred Westph, and Caiçara2	20	02/187	72/283	18/096	0.57 : -0.29 : -0.29			0.00	20	06/187	83/342	03/097	0.73 : -0.03 : -0.71		0.47	20
G Compilation from sites Pedr Guerra, CODECA1, Aflor Tega, and Veranópolis	11	02/076	84/328	06/166	0.59 : -0.25 : -0.34			0.10	25	01/072	88/324	02/162	0.79 : -0.02 : -0.77		0.48	30
H Pedr CODECA1	9	13/184	76/030	06/275	0.50 : -0.12 : -0.38			0.30	40	02/001	82/105	08/270	0.73 : -0.04 : -0.69		0.46	33
I Pedreira Paniel	10	13/002	76/208	06/094	0.52 : -0.17 : -0.35			0.20	25	03/008	87/198	01/098	0.72 : 0.01 : -0.72		0.51	39

7 Results for the linear and multiple-slip methods of inversion are calculated by the T-TECTO 3.0 program, according to Žalohar and Vrabc
8 (2007, 2008).

9

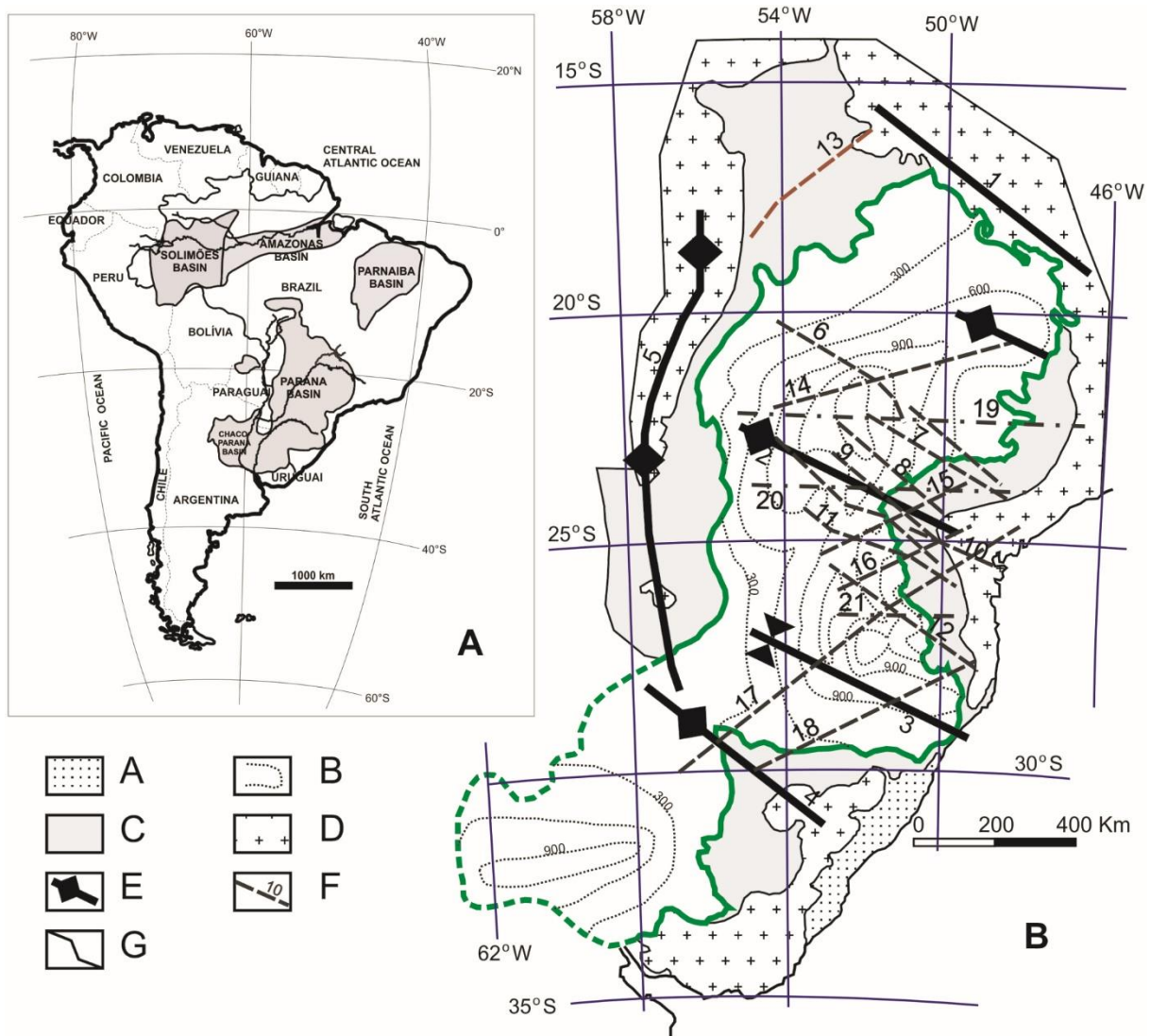
10 Table 6 Summary of principal stress axis in the NE–SW orientation computed for sites within the volcanic rocks of the Paraná Basin.

Site	Standard deviation of s	Linear inversion							MSM inversion				
		σ_1	σ_2	σ_3	Relative values of λ_i	D	ϕ_2	σ_1	σ_2	σ_3	Relative values of λ_i	D	ϕ_2
A Compilation from Pedr Sta Rita 1 + BR293 + Pedr Quarai 1	13	02/027	84/135	06/297	0.62 : -0.27 : -0.36 1.06 : 0.17 : 0.08	0.10	25	02/036	87/165	03/306	0.97 : -0.03 : -0.94	0.48	30
B Pedreira Sta Rita 2	11	02/309	84/201	06/040	0.65 : -0.27 : -0.37 1.10 : 0.18 : 0.08	0.10	25	04/113	85/337	04/203	0.82 : 0.01 : -0.83	0.51	35
C Pedreiras BR290 + BR377	16	02/223	72/320	18/133	0.57 : -0.19 : -0.38 1.06 : 0.30 : 0.11	0.20	25	08/039	80/254	06/130	1.03 : -0.10 : -0.92	0.42	25
D Compilation from sites Barragem M Filho and Gar Ralph	12	02/236	84/127	06/326	0.51 : -0.12 : -0.40 1.01 : 0.38 : 0.10	0.30	33	07/242	83/058	00/152	0.88 : -0.01 : -0.87	0.49	33
E Pedreira Dacito	16	13/142	76/296	06/051	0.65 : -0.28 : -0.39 1.11 : 0.18 : 0.08	0.10	30	04/143	72/247	17/052	1.03 : -0.21 : -0.82	0.33	32
F Compilation from sites Pedreiras FrWestph1, Caiçara1, RodBon1, and Planalto-Alpestre	16	02/125	84/234	06/035	0.57 : -0.19 : -0.38 1.05 : 0.29 : 0.10	0.20	30	04/126	85/273	03/036	0.98 : -0.04 : -0.93	0.47	25
G Pedreria Rodeio Bonito 2	8	13/058	76/264	06/150	0.52 : -0.12 : -0.39 1.01 : 0.37 : 0.10	0.30	33	15/040	75/230	02/131	0.96 : 0.04 : -1.00	0.53	40
H Rota dos Canions (RS)	18	02/039	84/148	06/309	0.57 : -0.19 : -0.38 1.06 : 0.30 : 0.11	0.20	30	09/041	81/216	01/310	1.02 : -0.08 : -0.95	0.44	30
I Compilation from sites Pedreiras BJSerra and Painel2	10	12/212	76/057	06/303	0.52 : -0.12 : -0.39 1.01 : 0.37 : 0.10	0.30	35	06/213	84/057	02/303	0.91 : 0.04 : -0.95	0.53	35

11 Results for the linear and multiple-slip methods of inversion are calculated using the T-TECTO 3.0 program, according to Žalohar and Vrabec

12 (2007, 2008).

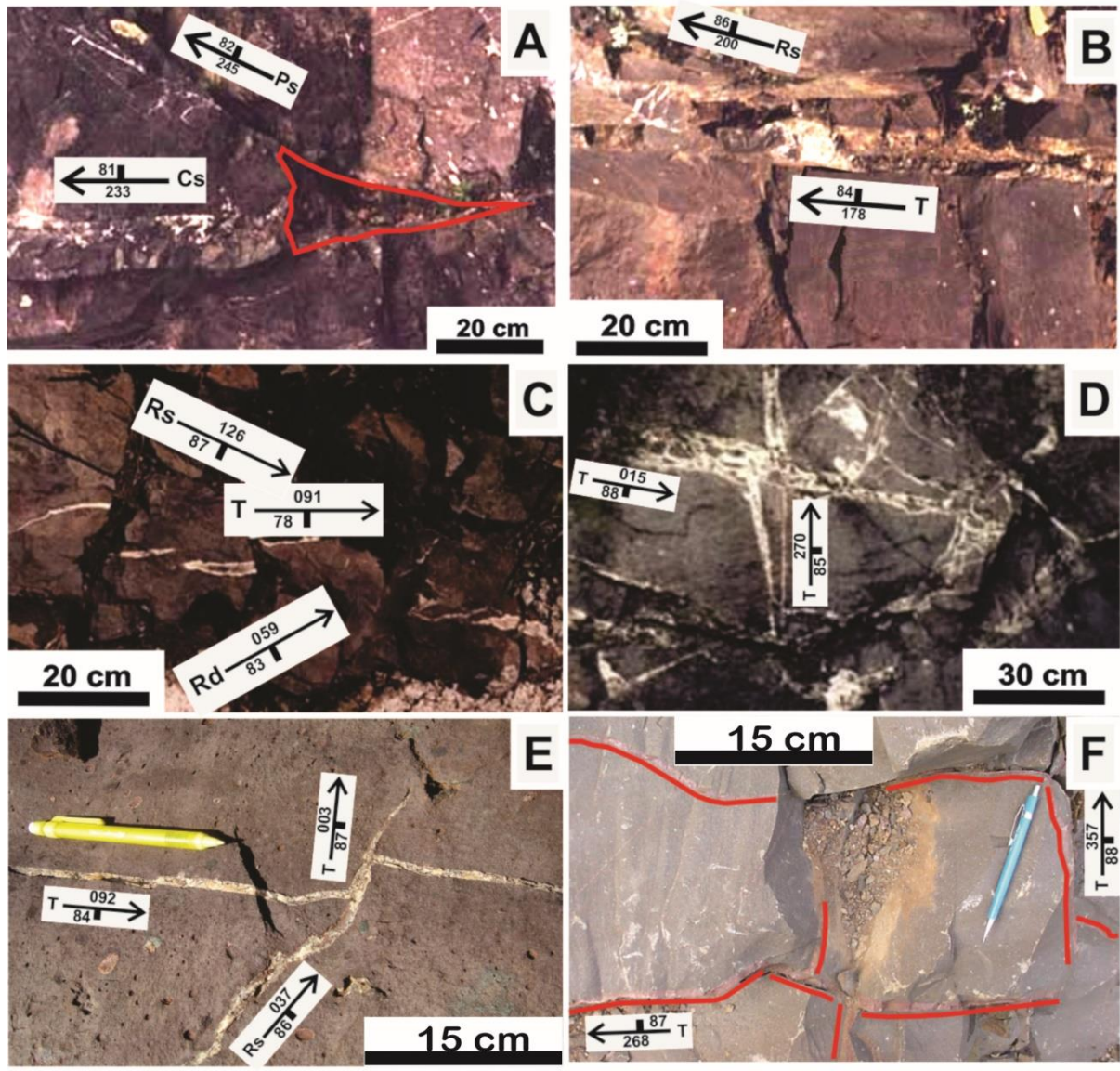
13 **Figures**



14
 15 Figure 1 A) Location of the Paleozoic–Mesozoic intracratonic basins of the South American
 16 continental plate (modified from Zalán et al. 1991); Chaco–Paraná Basin is actually covered
 17 by Tertiary and Quaternary sediments. B) Geological sketch of the Paraná Basin and its main
 18 structural features (modified from Leinz et al. 1968; Zalán et al. 1991). Legend: A)
 19 Quaternary sediments. B) Serra Geral Fm.; dotted lines show the actual thicknesses of the
 20 volcanic rock piles. C) Paleozoic to Mesozoic sedimentary rocks. D) Basement rocks. E)
 21 Structural highs, arches, and synclines. F) Main fault zones (numbered): 1) Alto Parnaíba
 22 high; 2) Ponta Grossa Arc; 3) Torres Syncline; 4) Rio Grande Arc; 5) Asunción Arc; 6)
 23 Guapiara; 7) Santo Anastácio; 8) São Jerônimo–Criúva; 9) Rio Alonso; 10) Cândido de

24 Abreu–Campo Mourão; 11) Rio Piquiri; 12) Caçador; 13) Transbrasiliano; 14) Araçatuba; 15)
25 Guaxupé; 16) Jacutinga; 17) Lancinha–Cubatão; 18) Blumenau–Soledade; 19) Mogiguaçu–
26 Dourados; 20) São Sebastião; 21) Taquara Verde. G) Main rivers.

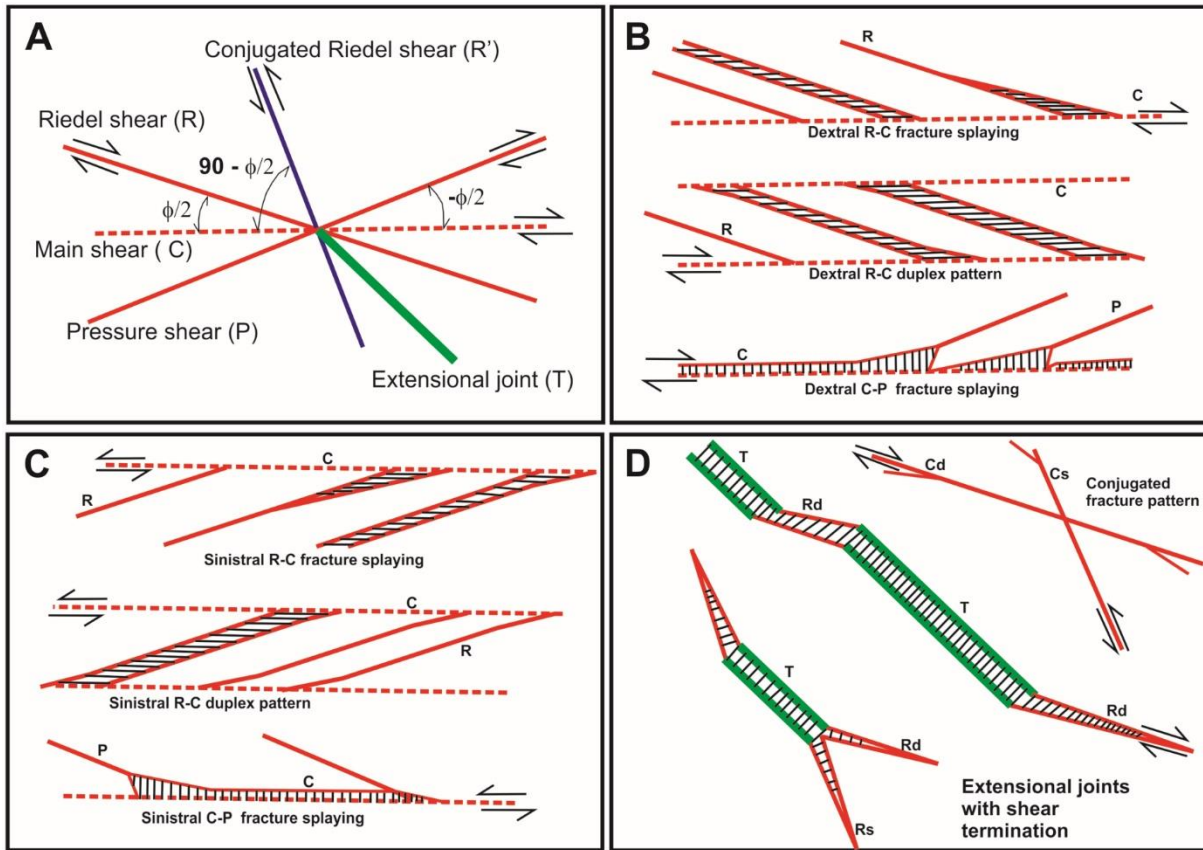
27



29

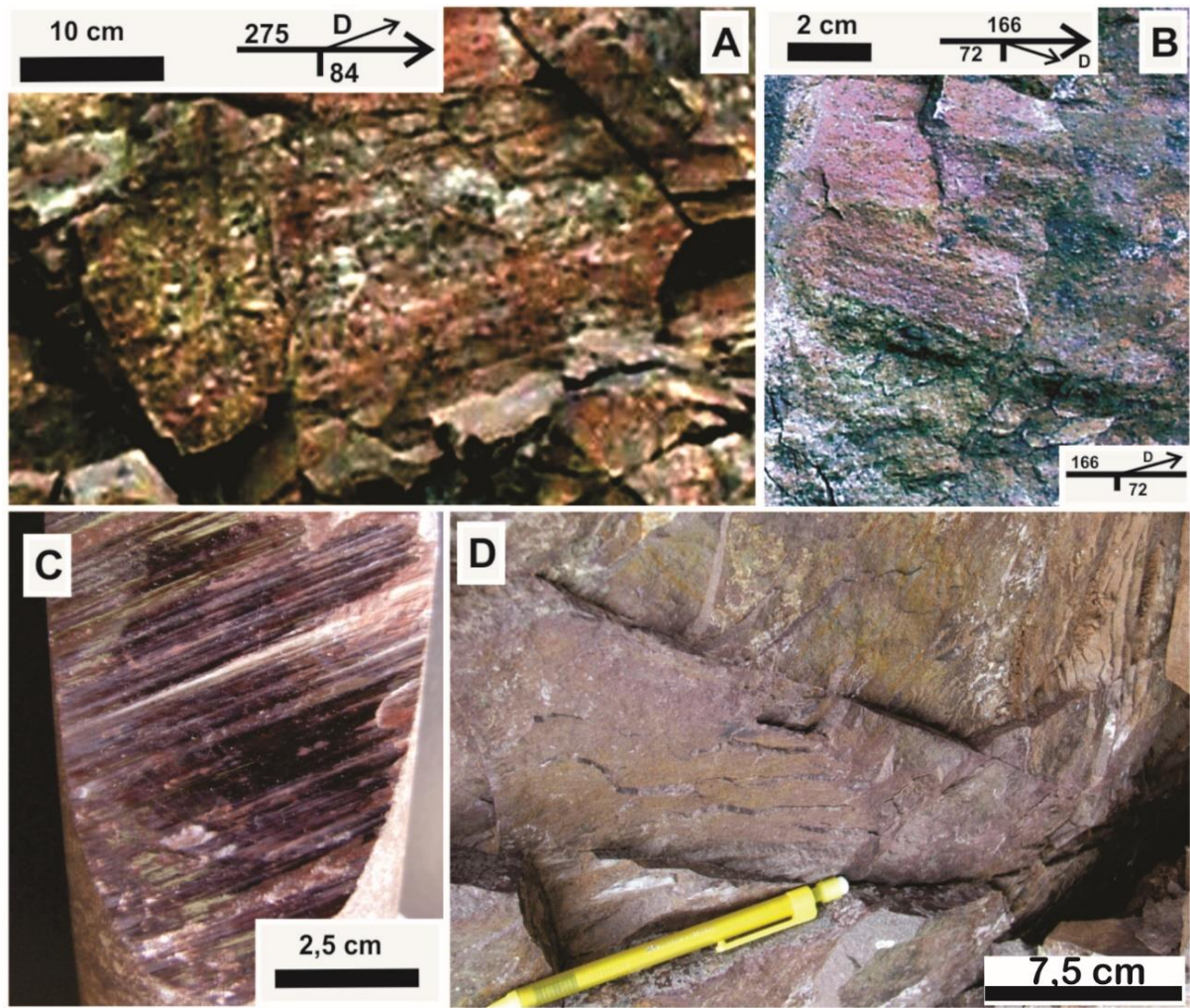
30 Figure 2 Fracture patterns in the Serra Geral Fm. volcanic rocks. A) Fracture splay and a
 31 triangular zone showing hydraulic breccia (weathered). B) Extensional joint terminating into
 32 R shear and hydraulic breccia. C) Extensional joints terminating into either dextral or sinistral
 33 shear. D) Different generation of extensional joints and hydraulic breccia. E) Orthogonal
 34 extensional joints filled by thermally metamorphosed sandstone. F) Orthogonal extensional
 35 joints filled by metamorphosed sandstone (the sandstone dykes were laterally delineated). R,
 36 C, and P are synthetic shear fractures; R' indicates antithetic shear; T indicates extensional

37 joints; **s** or **d** indicate sinistral or dextral fracture sense of movement, respectively. Notation
 38 for fracture orientation follows Fig. 3.
 39



40
 41 Figure 3 Field diagrams of fracture patterns in the volcanic rocks of the Serra Geral Fm. A)
 42 Riedel-type fractures, as reported by Tchalenko (1970) and Tchalenko and Ambraseys (1970).
 43 B) Dextral patterns of shear fractures. C) Sinistral patterns of shear fractures. D) Conjugated
 44 shear fractures and combinations of tension joints and shear fractures. Hatched areas represent
 45 transtensive dilatational spaces developed by shearing. R, C, and P are synthetic shear
 46 fractures; R' indicates antithetic shear; T indicates extensional joints; **s** or **d** indicate sinistral
 47 or dextral fracture sense of movement, respectively.

48
 49

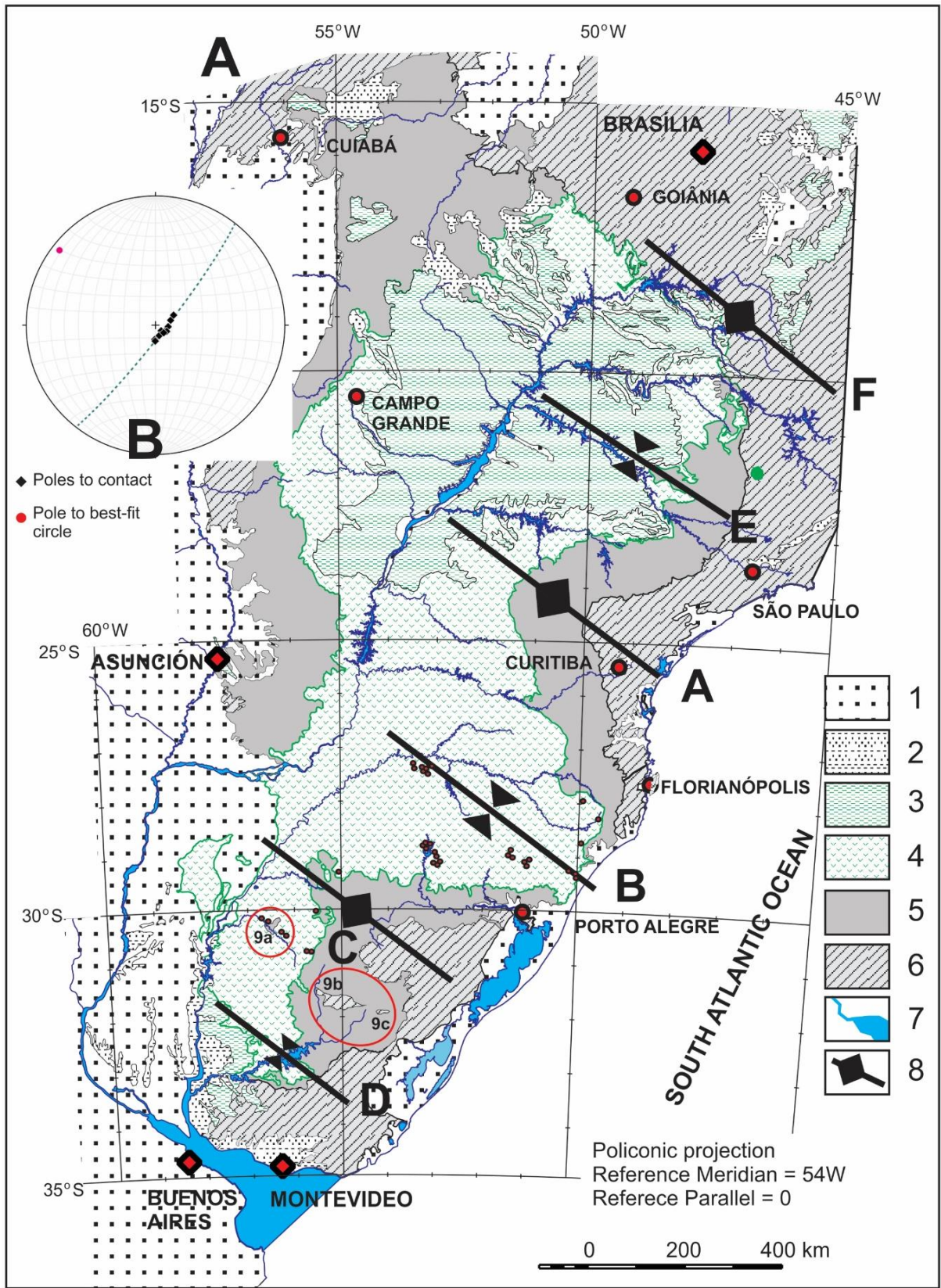


50

51 Figure 4 Geological features of the fault planes in the volcanic rocks of the Paraná Basin. A)
 52 RM-type striation. B) Overprinting of TM striation on former striation with mineralization in
 53 the same fault plane. C) Frictional striae and steps in a polished fault plane. D) Sub-
 54 centimeter fracture cleavage dragging the horizontal joints of basalt.

55

56

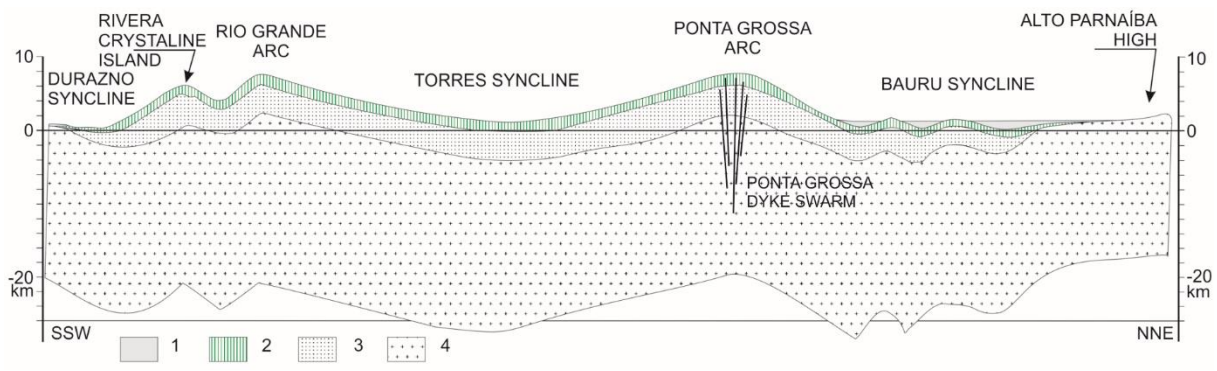


57

58 Figure 5 Regional folds developed by NE-SW paleostress tensors. A) Map showing the
 59 location of synclines and anticlines (arcs), and also the domes and basins in the southern part

60 of the Paraná Basin. B) Lower hemisphere, equal area stereogram of the basal contact of the
 61 Serra Geral Fm. along the Rio Grande Arc and Torres Syncline (dashed line is the best-fit
 62 great circle to poles). 1) Quaternary sediments. 2) Cenozoic sedimentary rocks. 3) Cretaceous
 63 to Paleogene sedimentary rocks. 4) Paraná Flood Basalts. 5) Paleozoic–Mesozoic sedimentary
 64 rocks of Paraná Basin. 6) Basement rocks. 7) Main rivers, lakes, and lagoons. 8) Main NW-
 65 oriented arcs and synclines. 9) Elongated domes (red circles do highlight): a) Quaraí Dome
 66 (see Fig. 7 for a detailed map), b) Rivera Crystalline Island, c) Aceguá Crystalline Island.
 67 Based on South America Geological Map (Schobbenhaus and Bellizzia 2001). Small open
 68 dots represent outcrops where fault-slip data were measured and analyzed.

69

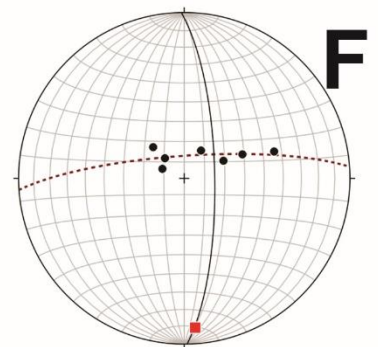
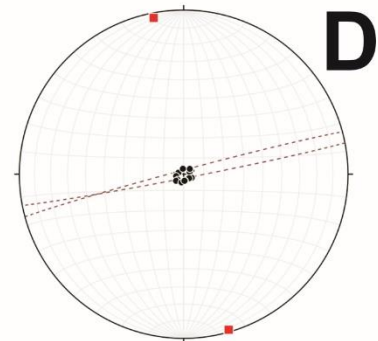
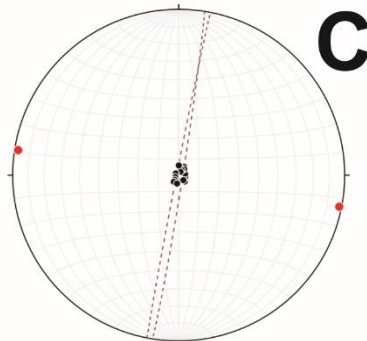
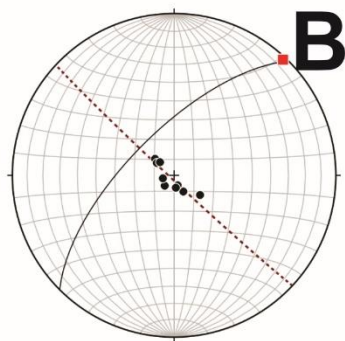
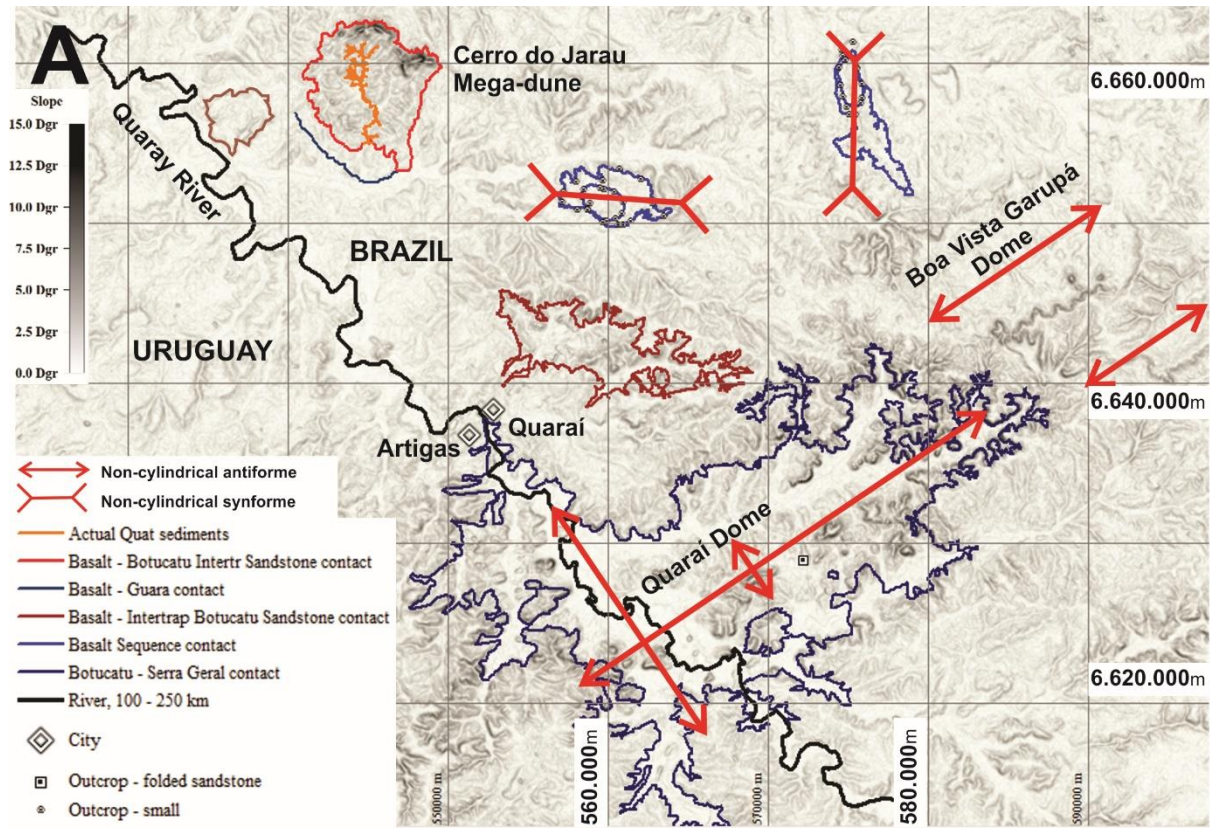


70

71 Figure 6 Balanced SW–NE cross section from Uruguay to São Paulo (Brazil) showing the
 72 gentle anticlines and synclines dipping NW in the eastern border of the Paraná Basin. The
 73 cross section is perpendicular to the fold hinge. 1) Cretaceous to Paleogene sedimentary
 74 cover. 2) Serra Geral Fm. 3) Paleozoic–Mesozoic sedimentary rocks of the Paraná Basin. 4)
 75 Basement. The structural section was built upon the South America Geological Map
 76 (Schobbenhaus and Bellizzia 2001), and structural field data. The vertical exaggeration is
 77 13×.

78

79



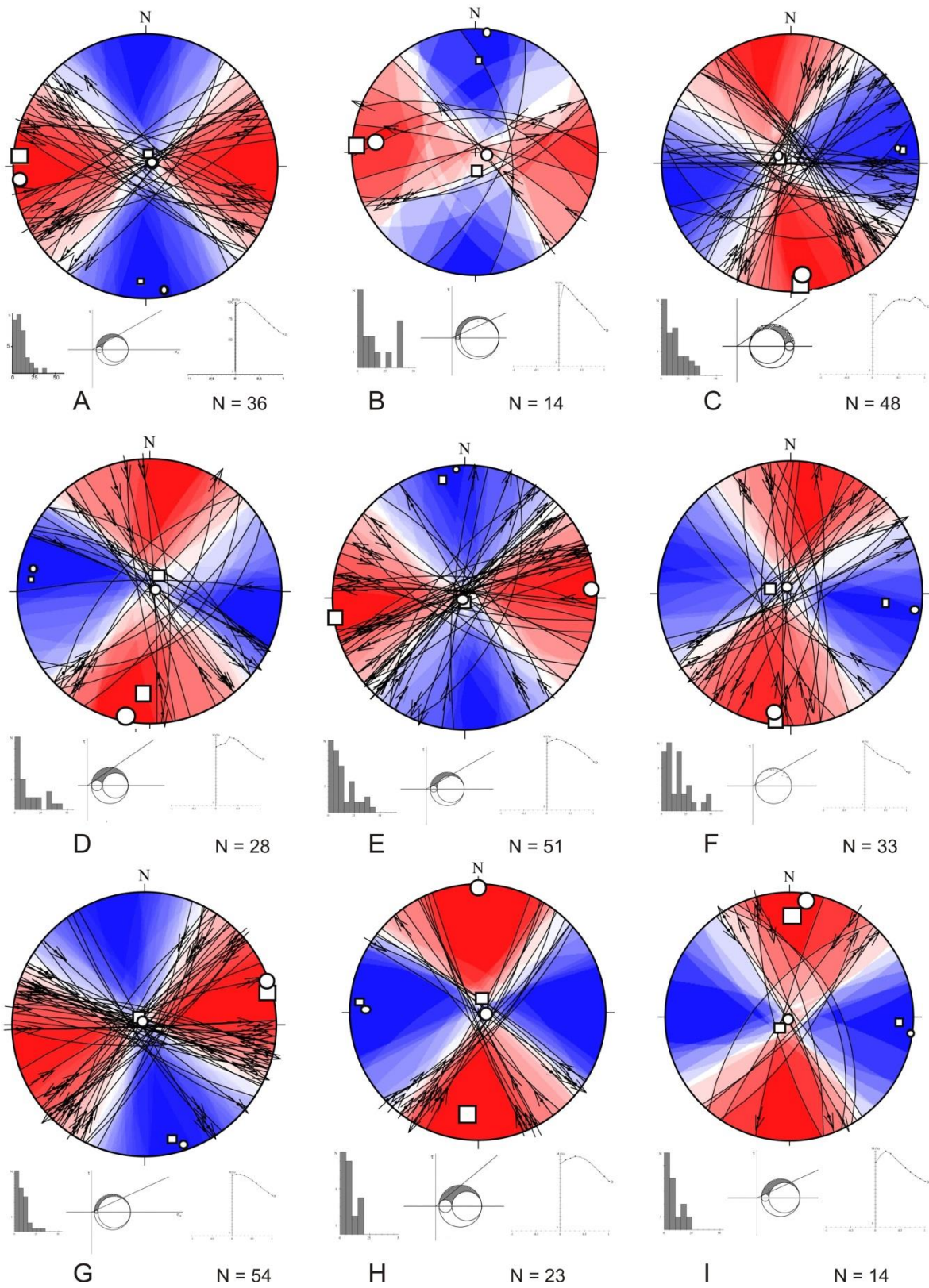
◆ Poles to contact
 ● Pole to best-fit circle

80

81 Figure 7 Dome and basin structures in the Quarai Dome area. A) Geological sketch indicating

82 the main structural features in the region. B) π diagram for sandstone-basalt contact in the

83 Quaraí Dome. C) π diagram for a basalt flow contact along the E–W basin. D) π diagram for
84 the basalt flow contact along the N–S basin. E) South-dipping fold in Botucatu Fm.
85 sandstone. F) π diagram for sandstone in the road cut outcrop. [\(Dashed lines in stereograms](#)
86 [are best-fit great circle to poles; continuous lines are axial plane to folds\).](#)
87

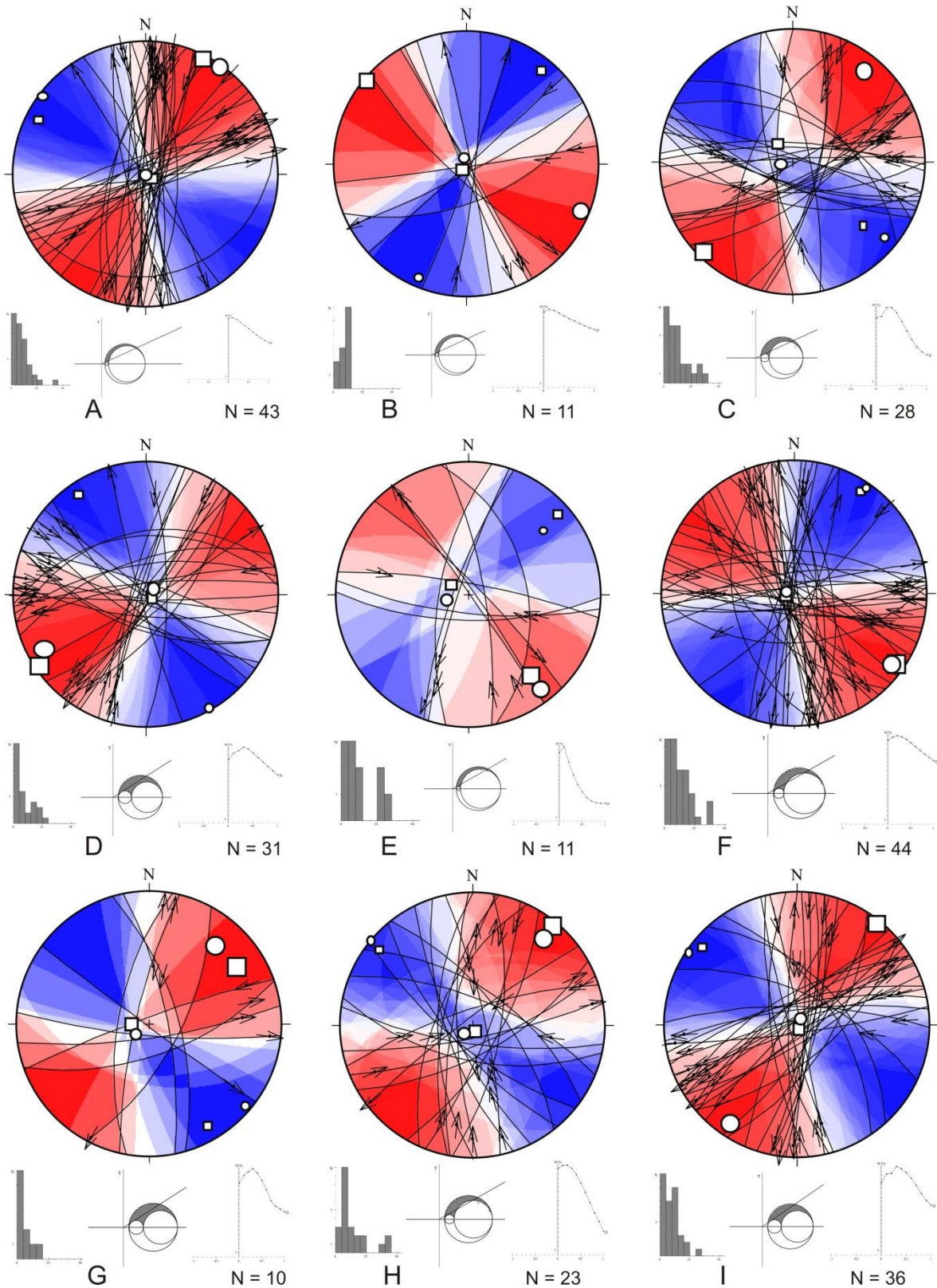


89

90 Figure 8 Paleostress results for the N-S and E-W tensors observed in the volcanic rocks of

91 the Paraná Basin. Each area/site is identified by a capital letter. The graphics for each area/site

92 include: lower hemisphere, equal area stereogram of brittle fault-slip data; misfit angle
93 histogram; Mohr diagram for resolved shear stress; and biplot of the value for object function
94 (M) vs. shape of the strain ellipsoid (D). Open circles and open squares in the stereograms
95 represent stress direction determined using the Gauss and MSM methods, respectively. The
96 sizes of the open circles and squares relate to the magnitudes of the stress tensors. The
97 stereograms show the fault planes and their respective striae and sense of movement. Red and
98 blue areas of stereograms represent P and T fields according Angelier and Mechler (1977),
99 respectively.
100



101

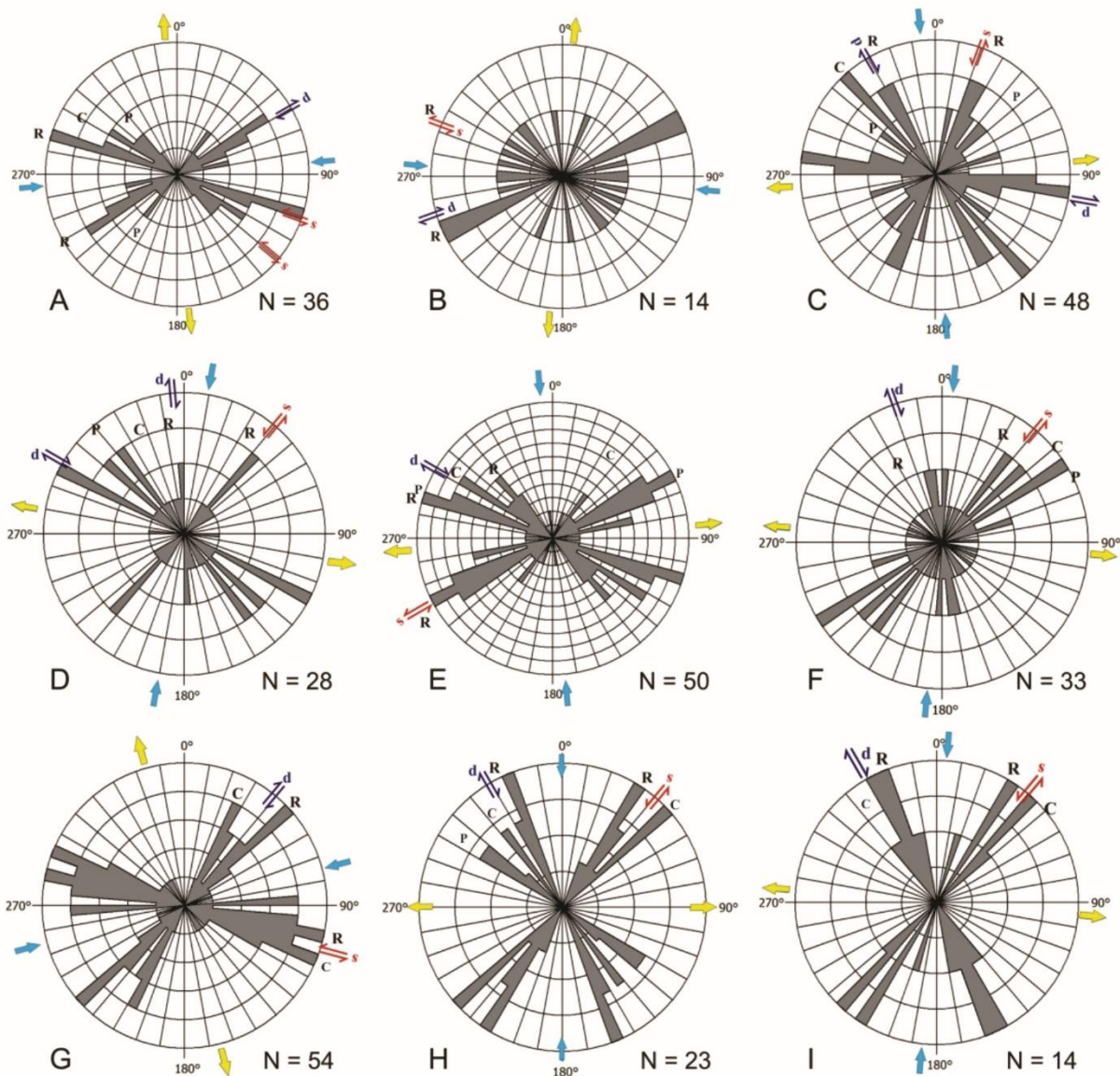
102 Figure 9 Paleostress results for NE–SW tensors observed in the volcanic rocks of the Paraná

103 Basin. Each area/site is identified by a capital letter. The graphics for each area/site include:

104 lower hemisphere, equal area stereogram of brittle fault-slip data; misfit angle histogram;

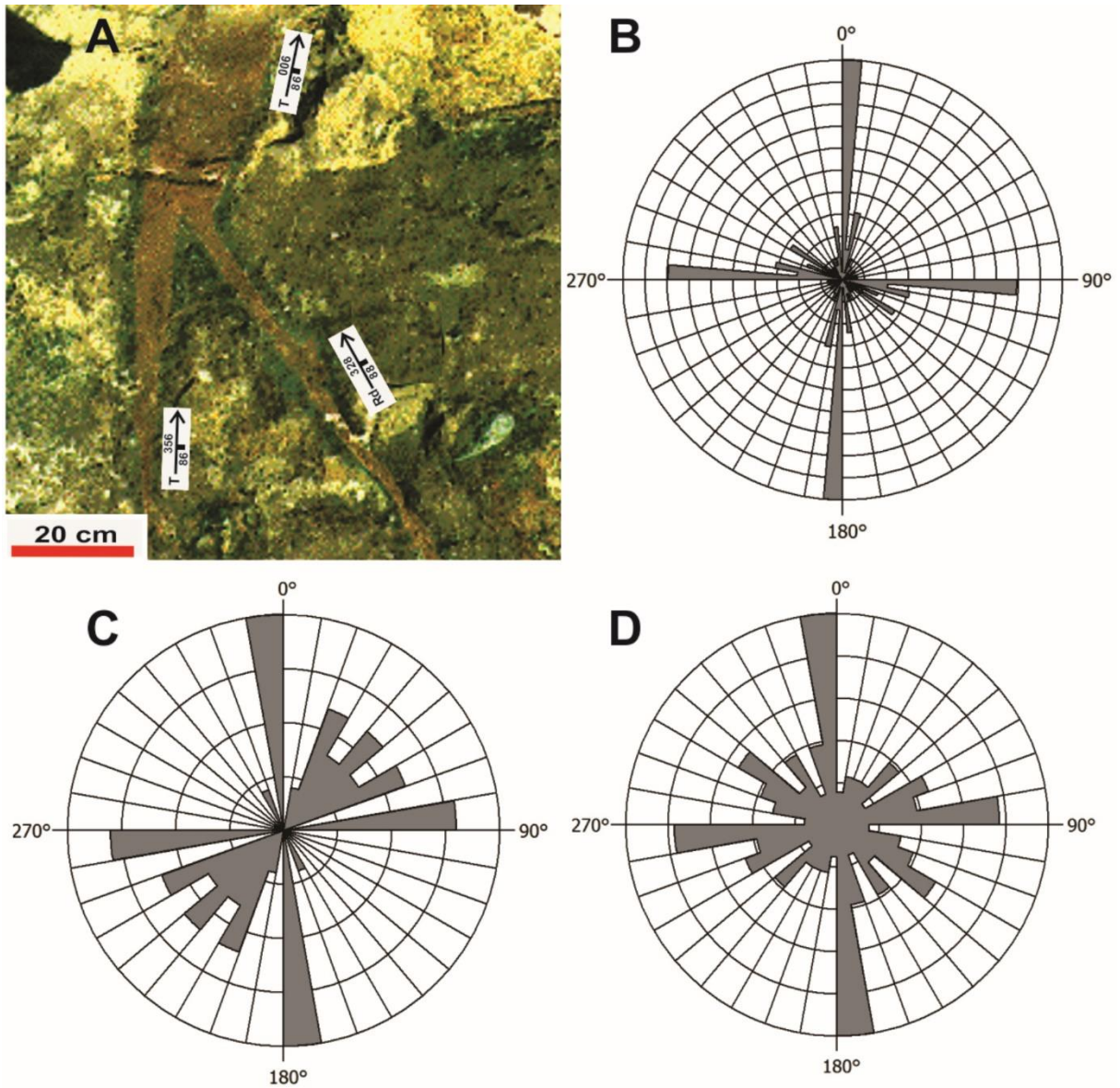
105 Mohr diagram for resolved shear stress; biplot of value for object function (M) vs. shape of
 106 the strain ellipsoid (D). Open circles and open squares in the stereograms represent stress
 107 direction determined using the Gauss and MSM methods, respectively. The sizes of the open
 108 circles and squares relate to the magnitudes of the stress tensors. [The stereograms show the](#)
 109 [fault planes and their respective striae and sense of movement. Red and blue areas of](#)
 110 [stereograms represent P and T fields according Angelier and Mechler \(1977\), respectively.](#)

111



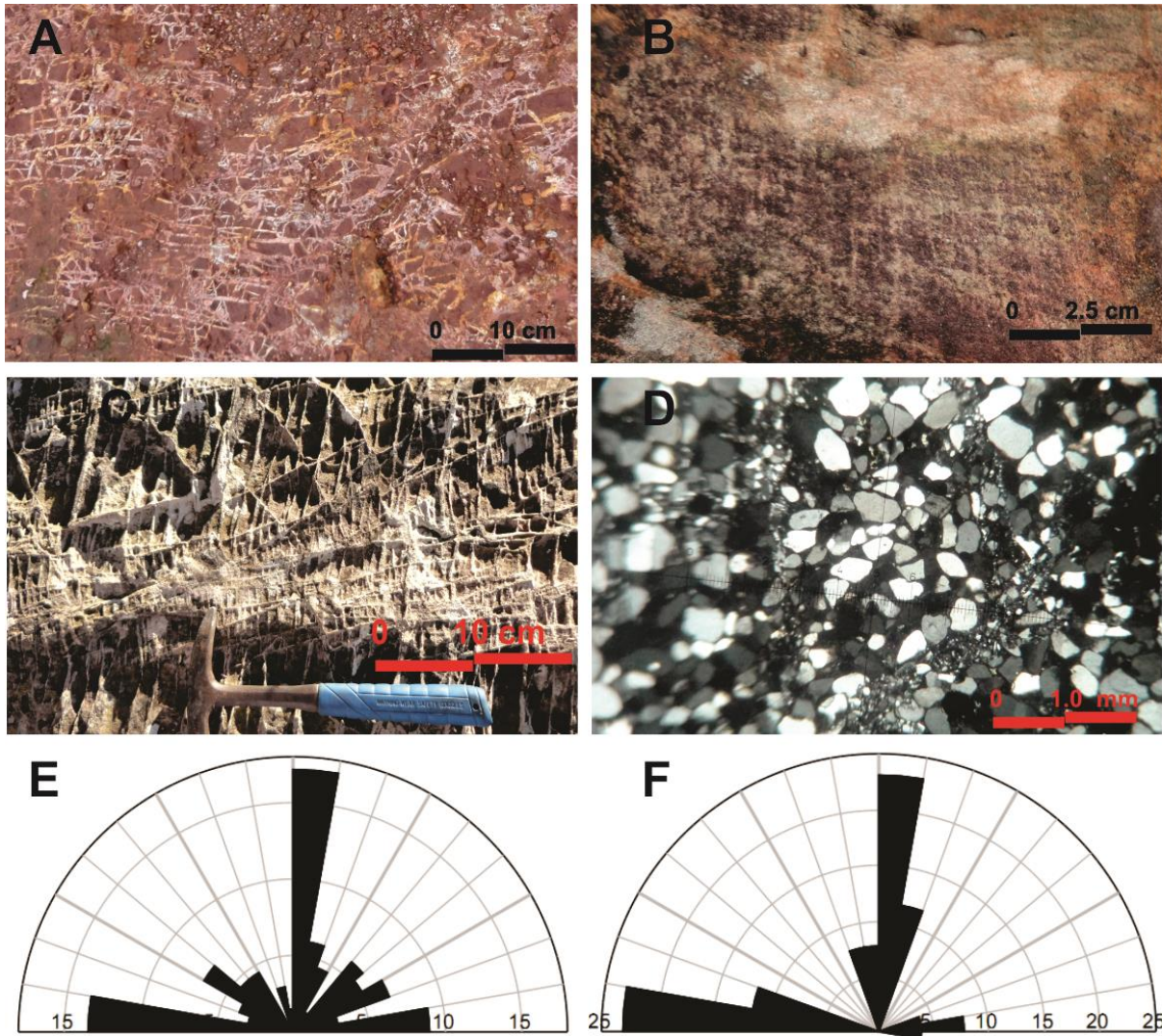
112

113 Figure 10 Rose diagrams of fault-slip data for N–S tensors. Circular histograms from A to I
 114 correspond to the sites/areas described in Table 3. [Blue and yellow arrows represent](#)
 115 [maximum and minimum stress tensor orientation from Fig. 8.](#)
 116
 117



118
 119 Figure 11 Tabular dykes emplaced into basalts of the Serra Geral Fm. A) Photograph of the
 120 tabular dykes emplaced into the vesicular basalts of the Salto do Jacuí region. B) Rose
 121 diagram of orientation of sandstone dykes in the Salto do Jacuí region (N = 135). C) Rose

- 122 diagram of orientation of sandstone dykes in the Caxias do Sul region (N = 24). D) Rose
- 123 diagram of orientation of mineralized veins in the Caxias do Sul region (N = 85).
- 124
- 125

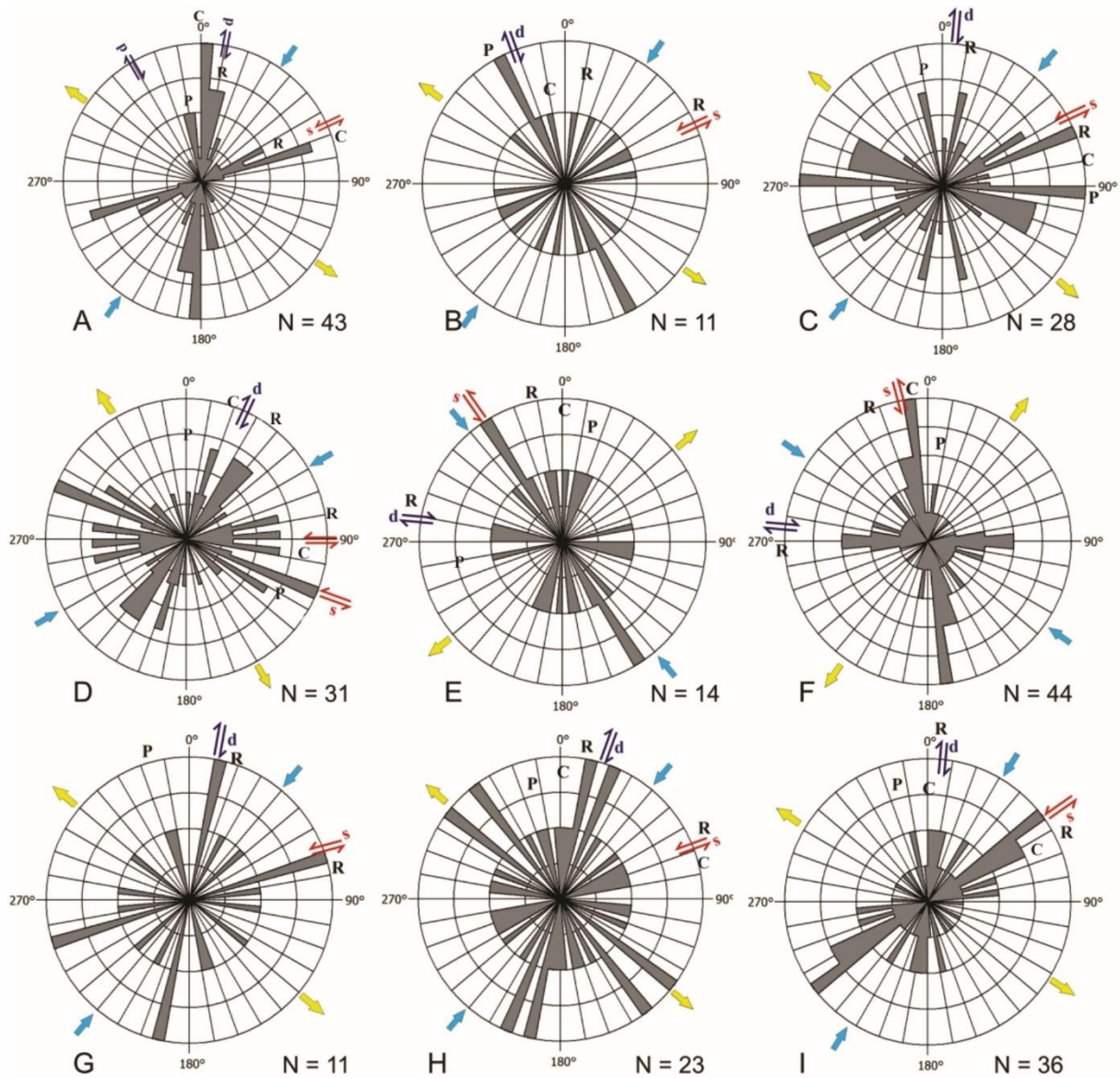


126

127 Figure 12 Orthogonal pattern features recorded in the Cerro do Jarau intertrap megadune. A)
 128 Centimeter-scale orthogonal “ladder-type” veins in the basalt of the Cerro do Jarau hills. B)
 129 Millimeter-scale orthogonal “grid-type” deformation bands in the Botucatu Fm. sandstone in
 130 the Cerro do Jarau intertrap dune. C) Superposed shear deformation bands on orthogonal
 131 bands. D) Thin section of thermally metamorphosed sandstone showing the orthogonal
 132 deformation bands. E) Rose diagram of the orthogonal veins in basalts (N = 134). F) Rose
 133 diagram of deformation bands in sandstones (N = 28).

134

135



136

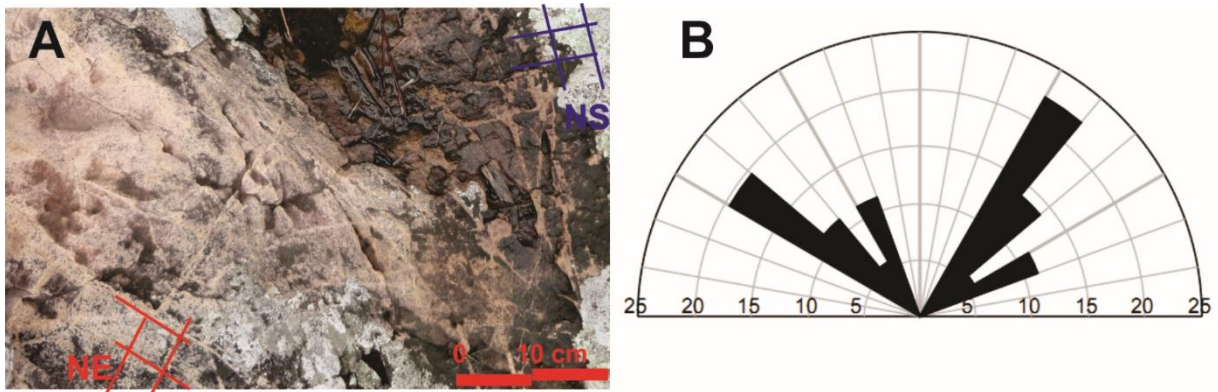
137 Figure 13 Rose diagrams of fault-slip data for NE–SW tensors. Circular histograms from A to

138 I correspond to sites/areas described in Table 4. [Blue and yellow arrows represent maximum](#)

139 [and minimum stress tensor orientation from Fig. 9.](#)

140

141



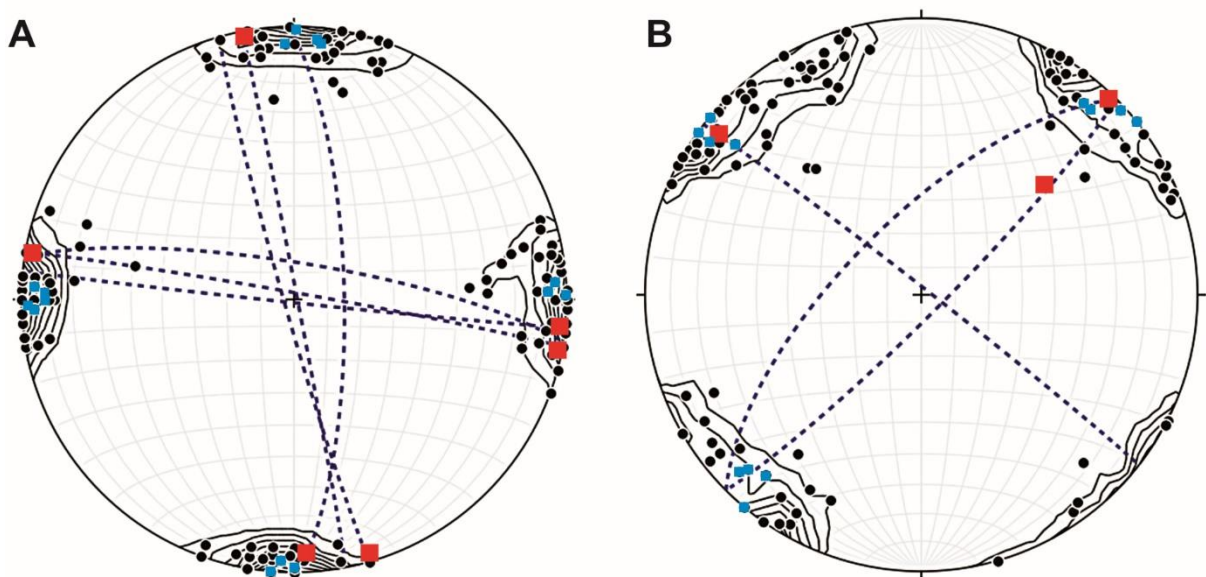
142

143 Figure 14 Orthogonal patterns associated with second deformational phase in the Cerro do

144 Jarau area. A) NE–SW orthogonal deformation bands superposed upon the N–S bands. B)

145 Rose diagram of the NE–SW orthogonal deformation bands (N = 36).

146



147

148 Figure 15 Lower hemisphere stereograms showing the symmetry relationships between

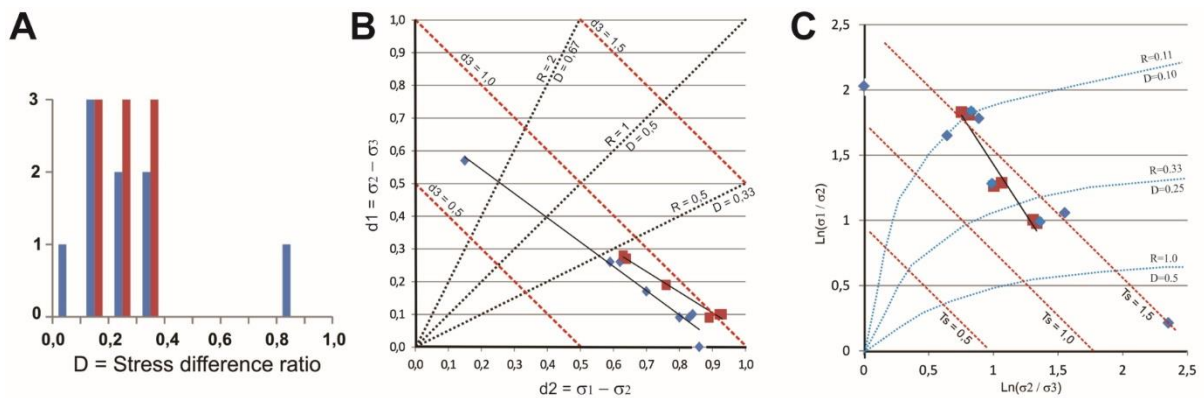
149 domes and basins and fractures in the Paraná Basin volcanics. A) Fold axis ([red squares](#)),

150 extensional dykes and veins ([blue squares](#)), and deformation bands ([black dots](#)) of the first

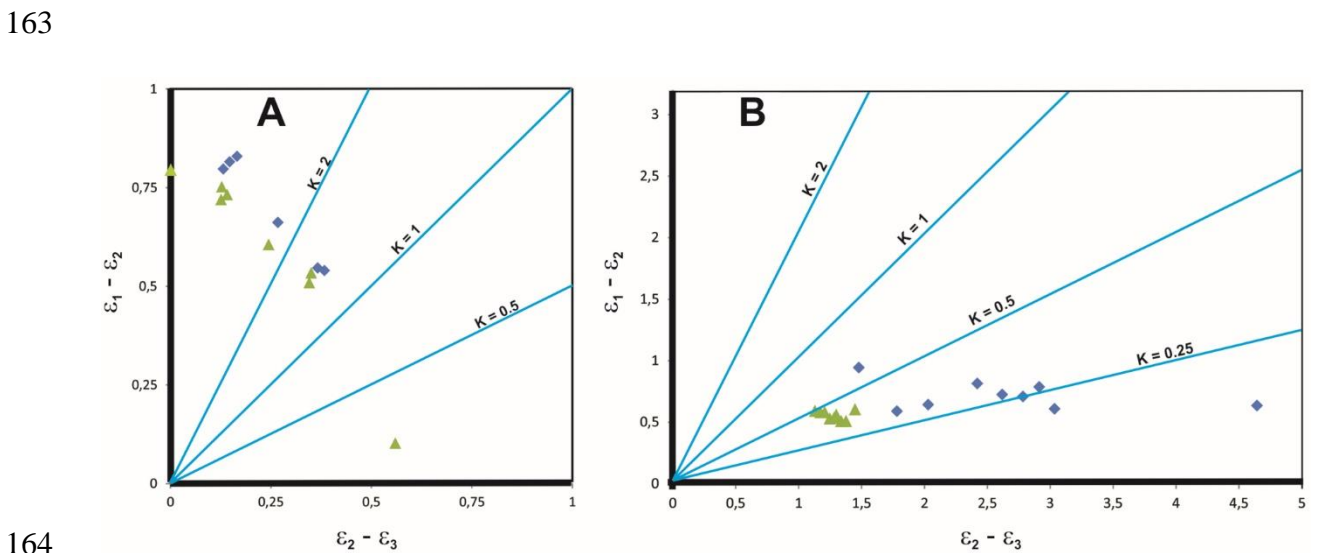
151 deformational phase in the Quaraí Dome area. B) Fold axis ([red squares](#)) for NW regional

152 arcs, Quaraí Dome, extensional dykes and veins ([blue squares](#)), and deformation bands ([black](#)

153 [dots](#)) of the second deformational phase. Dashed great circles are axial planes of folds and
 154 arcs.

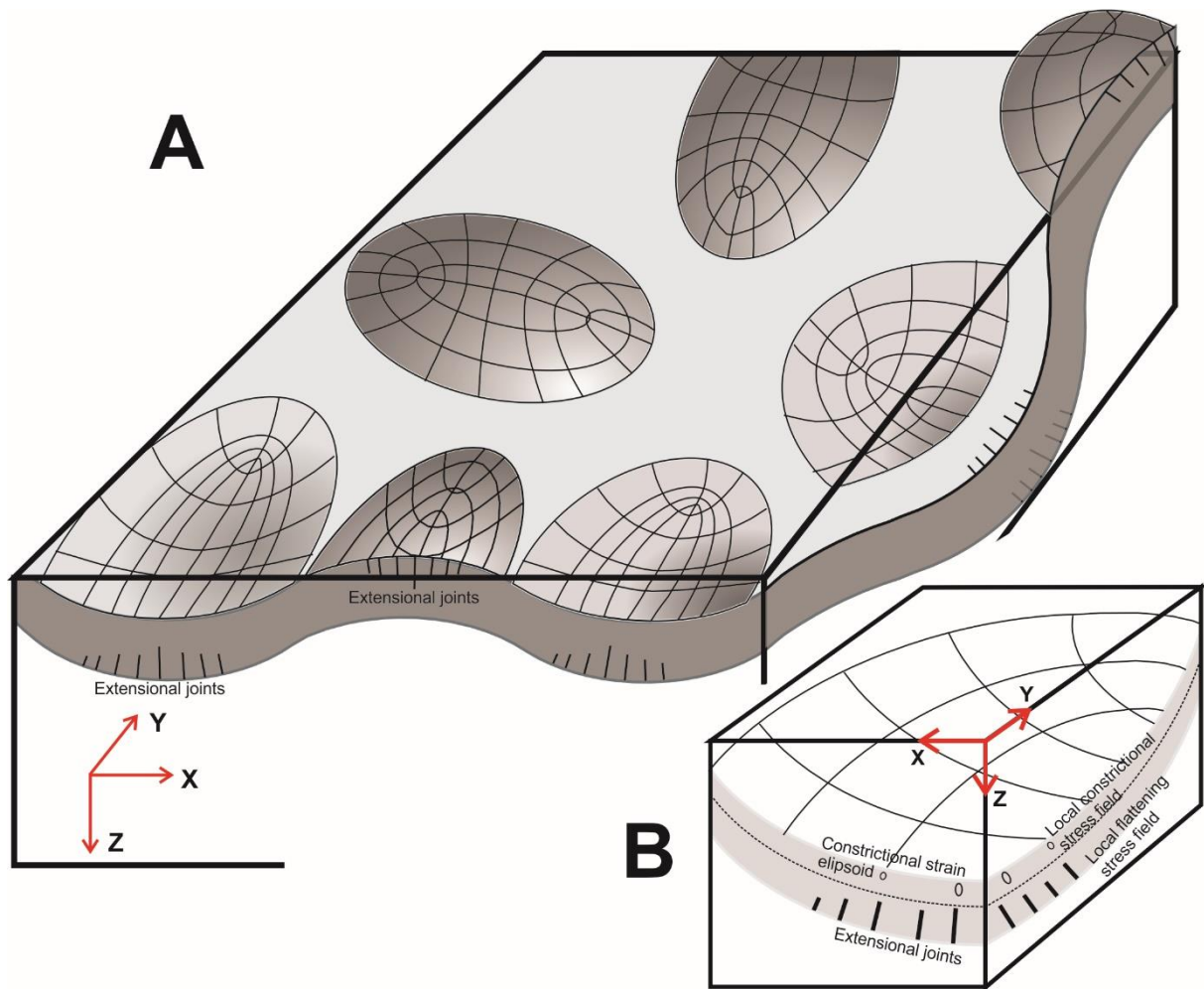


155
 156 Figure 16 Diagrams for stress states of the deformation phases in the Serra Geral Fm.
 157 volcanics, as determined by the linear inversion technique. A) Histogram for D values
 158 determined in each investigation area. B) Stress differences diagram of Lisle (1979). C) Stress
 159 ratio diagram of Morris and Ferrill (2009). Blue bars and diamonds represent N–S-oriented
 160 stress tensors. Red bars and squares represent NE–SW-oriented stress tensors. Thin black
 161 lines are the linear best fit for each paleostress regime. $R = d1/d2$ (Lisle 1979). $D = \Phi$
 162 (Angelier 1989). $R = D/(1-D)$.



164
 165 Figure 17 Strain-ratio log diagrams for volcanic rocks of the Paraná Basin. A) Results from
 166 the linear inversion method (Žalohar and Vrabc 2007). B) Results from multiple-slip method

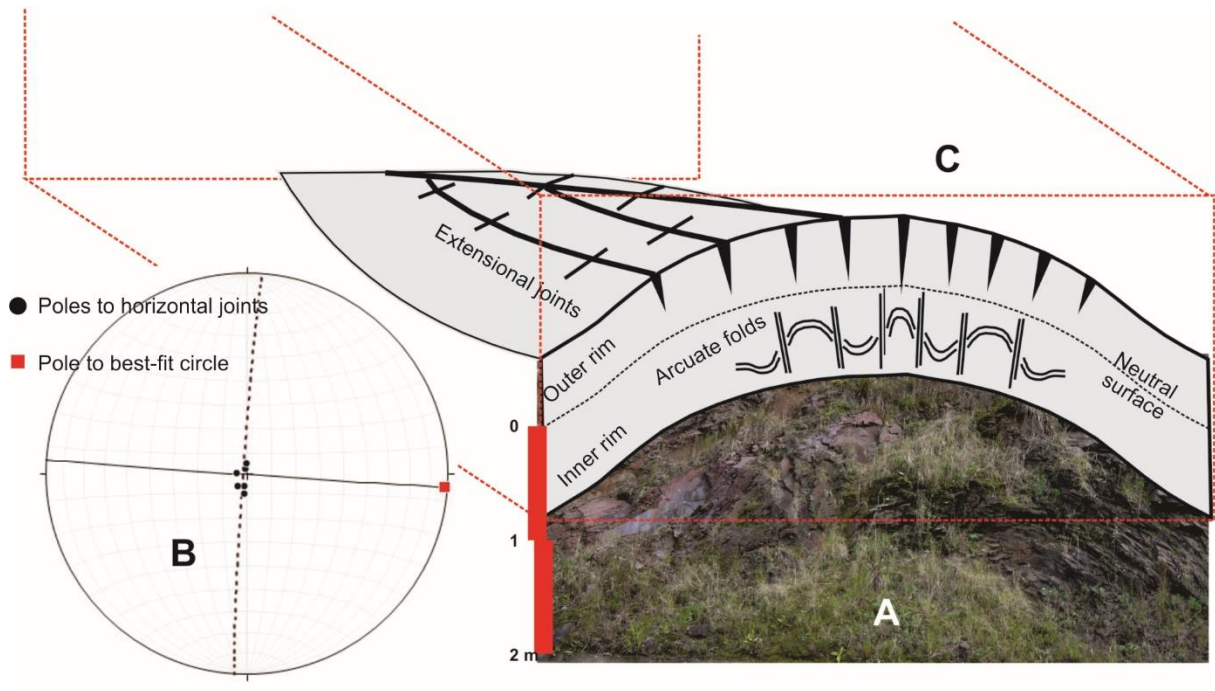
167 (Žalohar and Vrabc 2008). Green triangles represent the first deformational phase and blue
168 diamonds the second.



169

170 Figure 18 Bi-directional dome-and-basin model structures for the Serra Geral Fm. volcanics
171 (Paraná Basin). A) Regional sketch for orthogonal elliptical non-cylindrical folds. B) Detail
172 for local-scale stress/strain distribution in the tangential-longitudinal buckled volcanic layer;
173 stippled line distinguishes the neutral surface. The principal curvature directions (contour
174 lines for domes and basins) parallel to the principal strain directions give rise to orthogonal
175 joints in the outer rims of non-cylindrical folds (Lisle 1999).

176



177

178 Figure 19 Small-scale fold on basal horizontally jointed basalt flow. A) Outcrop-scale fold at
 179 base of a basalt flow. B) Lower hemisphere stereogram for folded horizontal joints of the
 180 basalt flow (Dashed lines in stereograms are best-fit great circle to poles; continuous lines are
 181 axial plane to folds). C) Tangential-longitudinal buckle model distinguishing structural
 182 features developed at the outer and inner rims of a buckled single layer flow.

183

184